

# Multi-objective energy management using a smart charging technique of a microgrid with the charging impact of plug-in hybrid electric vehicles

Amit Chakraborty <sup>\*</sup>, Saheli Ray

*Department of Electrical Engineering, National Institute of Technology Silchar, Silchar, Assam, India*



## ARTICLE INFO

**Keywords:**

Distribution generation  
Energy management  
Microgrid  
Net emission  
Operating cost  
Plug-in-hybrid electric vehicles

## ABSTRACT

The Microgrid (MG) concept is being developed to better integrate renewable energy sources and automate distribution networks. Microgrids combine distributed generating units (DGs) and energy storage systems to achieve this. This research paper aims to simultaneously minimize the daily operational cost and net environmental pollution of a small MG system, factoring in the charging demand from Plug-in-Hybrid Electric Vehicles (PHEVs) and consumer load demands. The proposed energy management process not only minimizes operational costs and emissions, but also determines the optimal battery size for the energy storage system. The analysis also explores the importance of two critical variables - the operation and maintenance costs of the DGs, and the total daily cost of the battery energy storage system. The demand for PHEV charging is managed using an intelligent charging approach. Given the complexity of the optimization, a recently developed metaheuristic algorithm, Slime Mould Algorithm (SMA), is applied. The performance of SMA is compared against the Grasshopper Optimization Algorithm and Sine Cosine Algorithm. To solve the multi-objective problem, a weighted sum method maintaining non-dominance and a fuzzy decision-maker technique are employed alongside the suggested algorithms. Three different scenarios verify the proposed method's effectiveness.

## 1. Introduction

In recent years, the use of RESs such as wind, biomass, solar, hydro, and others has gradually increased to fulfill high load demand, improve power quality, increase flexibility, lower cost, and reduce pollution emissions (Katiraei et al., 2008). MG constitutes a hosting environment designed to successfully manage and control RESs (Aghdam et al., 2020). Furthermore, in recent years, there has been a remarkable shift in focus from conventional vehicles to electric vehicles due to their potential to reduce reliance on fossil fuels such as petrol and diesel. When PHEVs become part of the power system, the proper management of energy within the MG becomes crucial in meeting the charging demands of their batteries (Ali et al., 2023). However, the stochastic nature of RESs adds complexity to the EM of an MG. The EM of an MG has recently gained popularity as a research domain Sedighzadeh et al. (2020). This section will first address the literature survey, second discuss the contributions, and third outline the organization of the article. In-depth research into optimization techniques, particularly those aligned with eco-friendly and sustainable economic principles, offers numerous benefits for the operational efficiency and EM of MGs. Moghaddam et al.

(Moghaddam et al., 2011) put forward a multifaceted AMPSO method to lessen the operational price and emission synchronously for three different scenarios of an MG. Milovanovic et al. (Milovanović et al., 2022) fabricated a novel model to control an MG's EM to curtail pollution rates by applying the WHO. Kumar et al. (Kumar & Karthikeyan, 2024) have proposed a novel approach to optimal energy dispatching for microgrids, using GJO. The Bat algorithm, 0-MKH Algorithm, QOSIMBO-Q, and WOA are applied to estimate the MG's operational cost by keeping appropriate BESS (Bahmani-Firozi & Azizipanah-Abarghooee, 2014; Sharma et al., 2016; Sharma et al., 2018; Yin et al., 2021). Zandrazavi et al. (Zandrazavi et al., 2022) developed a viable multi-objective solution approach to minimize voltage deviations and total operating costs in MGs. Chen et al. (Chen et al., 2022) proposed a novel additive relative decision-making process that accounts for various uncertainties to optimize the EM in grid-tied multi-energy MGs. Aghajani et al. (Aghajani & Ghadimi, 2018) developed a method called MOPSO to lower an MG's operating costs and pollution at the same time. The PHEV charging need during an MG's EM was not taken into account in the earlier research studies. Kavousi-Fard et al. (Kavousi-Fard et al., 2014) proposed a unique probabilistic expert strategy using 0-KH optimization to analyze the impacts of PHEVs on maintenance scheduling

\* Corresponding author at: Research Scholar, Department of Electrical Engineering, National Institute of Technology Silchar, Silchar, Assam, India.  
E-mail address: [amit\\_rs@ee.nits.ac.in](mailto:amit_rs@ee.nits.ac.in) (A. Chakraborty).

Nomenclature	
AMPSO	Adaptive Modified Particle Swarm optimization
BESS	Battery Energy Storage System
BSO	Backtracking Search Optimization
CO <sub>2</sub>	Carbon Dioxide
DGs	Distributed Generators
EM	Energy Management
FC	Fuel Cell
EMPCT	Economic Model Predictive Control Tracking
GJO	Golden Jackal Optimization
GOA	Grasshopper Optimization Algorithm
GWO	Gray Wolf Optimization
GSA-PS	Gravitational Search and Pattern Search
MG	Microgrid
MOPSO	Multi-Objective Particle Swarm Optimization
MT	Micro-turbine
MSFLA	Modified Shuffled Frog Leaping Algorithm
NDA	Non-Dominated Approach
NO <sub>x</sub>	Nitrogen Oxides
PDF	Probability Density Function
PHEV	Plug-in-hybrid-electrical vehicle
PV	Photovoltaic Cell
QOSIMBO-Q	Quasi-Oppositional Swine Influenza Model-based Optimization with Quarantine
QPSO	Quantum Particle Swarm Optimization
RESs	Renewable Energy Sources
SMA	Slime Mould Algorithm
SCA	Sine Cosine Algorithm
SO <sub>2</sub>	Sulfur dioxide
VAC	Volts Alternating Current
WHO	Wild Horse Optimization
WOA	Whale Optimization Algorithm
WT	Wind Turbine
YAIIE	Yearly Amortized Initial Installation Expenditure
θ-MKH	θ-modified Krill Herd
θ-KH	θ-Krill Herd
f <sub>1</sub> , f <sub>2</sub>	Operational Cost, Emission
γ <sub>PHEV</sub>	Possibility of existing coefficient of PHEV.
τ	Time Index.
σ <sub>PHEV</sub> <sup>min</sup> /σ <sub>PHEV</sub> <sup>max</sup>	Minimum/ maximum hourly PHEV demand (kW).
σ <sub>PHEV</sub> (τ)	Hourly mean values of PHEV demand (kW).
θ <sub>m</sub> (τ)	Hourly cost of energy prices.
T	Period of a day per hour basis.
E:	Total energy consumption for PHEVs (kWh).
Cost <sub>G</sub> (τ)	Trade-related costs with the upstream grid at τ (€ct).
Cost <sub>DG</sub> (τ), Cost <sub>BESS</sub> (τ)	Power price for DGs and BESS at τ (€ct).
OCPD <sub>BESS</sub>	Overall daily cost of BESS
Startup_cost <sub>MT</sub> (τ), Startup_cost <sub>fuel</sub> (τ)	The start-up cost for MT and FC at the timer, respectively (€ct).
Shutdown_cost <sub>MT</sub> (τ), Shutdown_cost <sub>fuel</sub> (τ)	The shutdown cost for MT and FC at the time, respectively (€ct).
Bid <sub>G</sub> (τ), Bid <sub>MT</sub> (τ), Bid <sub>fuel</sub> (τ), Bid <sub>WT</sub> (τ), Bid <sub>PV</sub> (τ), Bid <sub>BESS</sub> (τ)	A bid rate of utility, MT, FC, WT, PV, BESS at the timer, respectively (€ct/kWh).
W <sub>grid,max</sub> , W <sub>grid,min</sub>	Maximum and minimum utility output power in kW.
Start_up <sub>MT</sub> , Start_up <sub>fuel</sub> , Shut_down <sub>MT</sub> , Shut_down <sub>fuel</sub>	Cost coefficients for MT and FC during startup and shutdown (€ct), respectively.
tax	Tax rate of the power price for the utility.
W <sub>G</sub> (τ), W <sub>MT</sub> (τ), W <sub>fuel</sub> (τ), W <sub>WT</sub> (τ), W <sub>PV</sub> (τ), W <sub>BESS</sub> (τ)	Power of utility, MT, FC, WT, PV, BESS, respectively (kW).
W <sub>Demand_load</sub> (τ)	Distribution side consumer demand
W <sub>MT,max</sub> , W <sub>fuel,max</sub> , W <sub>PV,t,max</sub> , W <sub>WT,t,max</sub> , W <sub>BESS,max</sub>	Maximum power output limit of MT, FC, PV, WT, and BESS, respectively (kW).
Δτ	Time interval duration.
η <sub>d</sub> , η <sub>c</sub>	Overall efficiency of BESS is a function of its charge and discharge characteristics
E <sub>BESS,min</sub> , E <sub>BESS,max</sub>	BESS's minimum and maximum sizes (kW h).
E <sub>BESS</sub> (τ)	Energy stored in the BESS at the time τ (kWh).
W <sub>discharge_rate<sub>BESS</sub>,t</sub> , W <sub>charge_rate<sub>BESS</sub>,t</sub>	Maximum discharge and charge rates of BESS at the time τ (kW).
U <sub>BESS</sub> (τ), U <sub>MT</sub> (τ), U <sub>fuel</sub> (τ)	Status (On or Off) of BESS, MT, and FC at the timer, respectively.
OM <sub>cost</sub> , OM <sub>cost<sub>MT</sub></sub> , OM <sub>cost<sub>fuel</sub></sub> , OM <sub>cost<sub>PV</sub></sub> , OM <sub>cost<sub>WT</sub></sub>	Fixed operation and maintenance cost of DG, MT, FC, PV, and WT, respectively (€ct/kWh).
Iter-Max	Maximum number of iterations.
t	Recent iteration number.
F_C	Fixed cost
MC	Maintenance cost
r	interest rate
l	lifetime of the BESS
ζ	Penalty factor

and monitoring techniques, without taking the whole daily costs of the BESS into account. References (Chen et al., 2011; Miao & Hossain, 2020) utilized GWO method and the mathematical programming language to determine the minimum operating cost by optimizing the energy use of different DGs in an MG. Li et al. (Li et al., 2021) evolved a framework to minimize the MG's entire functioning cost by applying a hybrid GSA-PS algorithm that apprehended all the PHEVs, loads, RESs, and instability of energy prices and modeled them for a whole day. Alarcón et al. (Alarcón et al., 2022) derived a control strategy based on an EMPCT for changing economic criteria by managing energy resources in a residential microgrid. This paper did not devise a plan for dealing with the random variables in the system. Fouladi et al. (Fouladi et al., 2020) suggested a smart charging strategy in the presence of RESs to reduce MGs' reliance on the main grid and lower their energy consumption from the utility. Alam et al. (Alam et al., 2015) broadened the regulated charging and discharging techniques that enhance the battery competence of PHEVs to upgrade grid support. Several algorithms have been

utilized for commercial or economic control of microgrid, accounting for the requirement of PHEVs charging, including MSFLA, θ-MKH, QPSO, and BSO (Aldosary et al., 2021; Li et al., 2021; Liu et al., 2022; Li et al., 2020). However, refs (Aldosary et al., 2021; Li et al., 2021; Liu et al., 2022; Li et al., 2020) did not consider OCPD<sub>BESS</sub> and OM<sub>cost</sub> costs during the time of economic control. Moreover, pollution emissions are also not controlled in these papers. The current research article fulfills all the gaps and develops a proper EM which is simultaneously beneficial in terms of economic and environmental perspectives. Key contributions of this article include:

- Simultaneous optimization of operating costs and emissions of a MG in the presence of PHEV charging demand for each of the three scenarios. Many studies, such as (Aldosary et al., 2021; Li et al., 2021; Kavousi-Fard et al., 2014; Liu et al., 2022; Li et al., 2021; Li et al., 2020), have focused on reducing only the operational cost of an MG with PHEV charging demand. Other studies,

including (Aghajani & Ghadimi, 2018; Kumar & Karthikeyan, 2024; Milovanović et al., 2022; Moghaddam et al., 2011; Zandazavi et al., 2022), have simultaneously optimized both operational cost and emission in an MG where PHEV is not included. However, to the authors' knowledge, no research has integrated these two research fields into a single framework, where an MG uses a robust EM process to simultaneously optimize both operational cost and emission in the presence of PHEV charging demand. This article also separately evaluates the operational cost and emission of an MG with PHEV charging demand as single objectives and compares the effective PHEV load distribution between single and multi-objective in each scenario. Additionally, this work considers the pollution emissions from the utility grid, making the proposed EM process more practical and efficient.

- ii) This article also contributes by considering  $OM_{cost}$  and  $OCPD_{BESS}$  when estimating the operational cost of an MG in the context of PHEV charging demand. Most articles, such as (Aldosary et al., 2021; Li et al., 2021; Kavousi-Fard et al., 2014; Liu et al., 2022; Li et al., 2021; Li et al., 2020), that address PHEV charging demand during the optimal EM process of MGs do not include  $OM_{cost}$  and  $OCPD_{BESS}$  parameters in the objective function for minimizing operational cost. The significance of  $OCPD_{BESS}$  is substantial, as the optimal size of BESS is determined based on it. To the authors' knowledge, the optimal size of the storage system and the importance of these two parameters have not been previously investigated in the presence of PHEV charging impact.
- iii) This article introduces the use of the recently developed SMA to control the EM of the MG, comparing its outcomes with methods like GOA and SCA. The authors address the multi-objective problem by integrating WSM, which preserves non-dominated conditions, with a fuzzy decision-making method for each algorithm. A smart charging strategy is implemented to manage PHEV demand, and three scenarios are examined to validate the proposed EM approach. This combination represents a novel method for tackling the multi-objective challenges of an MG with PHEV charging demand.

The modeling approach to control the need for PHEV charges is described in Section 2. The MG's operating cost is mathematically described in Section 3. Section 4 presents the use of SMA to simultaneously minimize the MG's operational cost and emissions. The simulation results are discussed in Section 5, and the conclusion of this research article is drawn in Section 6.

## 2. Modeling of smart charging strategy for PHEVs

PHEV energy storage systems have limited capacity, requiring quick-access charging stations. To address this, charging stations are being installed in public places and at the homes of PHEV owners (Eskandari et al., 2022). However, PHEV charging demand depends on various uncertain factors, leading to uncertain charging requirements at public stations and residential locations (Eskandari et al., 2022; Li & Zhang, 2012). A notable trend is that electric vehicle owners are charging their cars during peak hours. This can cause several grid-related issues, such as feeder congestion, increased power losses, reduced reliability, poor power quality, and transformer saturation (Kavousi-Fard et al., 2014). To address the grid-related issues caused by uncontrolled PHEV charging during peak times, a smart charging scheme is considered here. Smart charging allows for higher PHEV injection on the network compared to uncontrolled charging. In uncontrolled charging, PHEV charging occurs at arbitrary times. In contrast, a smart charging strategy allows PHEVs to charge themselves at the optimal time of day, based on the system's calculation of power pricing and excess amount of power. Weibull PDF and normal PDF are considered to mitigate the uncertainty of PHEV charging (Eskandari et al., 2022; Ghaedi et al., 2016; Rezaee

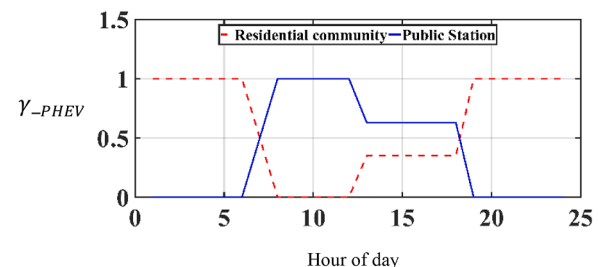


Fig. 1.  $\gamma_{PHEV}$  in charging points.

**Table 1**

Different types of charger data information.

Level type	1	2	3	4
Input voltage	120	280–240	280–240	280–600
VAC	VAC	VAC	VAC	VAC
Maximum power-kW	1.44	11.5	86	240

et al., 2013).

The suggested charging method uses two types of data: the total count of PHEVs at the charging station and hourly energy price data, with the intent to fulfill the demand for charging the PHEVs. Data on hourly energy prices in the market is collected using a widely used forecasting method. The possibility of a PHEV being present at a suitable charging station is denoted by an  $\gamma_{PHEV}$  in the second parameter. The values of  $\gamma_{PHEV}$  for public and home charging locations are displayed in Fig. 1 (Kavousi-Fard et al., 2014). Homeowners charge PHEVs overnight, as shown in Fig. 1. However, Fig. 1 also shows that PHEVs are charging at public stations during midday. The following computation controls the demand for PHEV charging (Kavousi-Fard et al., 2014).

$$\text{Minimize} \left( \frac{\theta_m(\tau)}{\gamma_{PHEV}} \times \sigma_{PHEV}(\tau) \right) \quad (1)$$

For the smart charging method:

$$\sum_{\tau=1}^T \sigma_{PHEV}(\tau) = E \quad \tau = 1, 2, 3, \dots, T \quad (2)$$

Here, the  $\sigma_{PHEV}(\tau)$  should lie in between  $\sigma_{PHEV}^{\min}$  and  $\sigma_{PHEV}^{\max}$  value.

$$\sigma_{PHEV}^{\min} \leq \sigma_{PHEV}(\tau) \leq \sigma_{PHEV}^{\max} \quad (3)$$

here, hourly energy prices are represented by  $\theta_m(\tau)$ . The average PHEV charging demand (kW) per hour is shown by  $\sigma_{PHEV}(\tau)$ . The hourly minimum and maximum PHEV demand (kW) are implied by  $\sigma_{PHEV}^{\min}$  and  $\sigma_{PHEV}^{\max}$ , respectively. "E" represents the PHEVs' total energy consumption (kWh). A variety of PHEV models are available, including the PHEV-20, PHEV-30, and others. However, this study specifically focuses on examining the PHEV-20 model. The charging rate according to charge level is provided in Table 1 (Li et al., 2021; Tao et al., 2021). This article covers residential and public charging stations with Level 1 and Level 2 chargers, although Level 3 and Level 4 chargers are related to commercial purposes. Levels 3 and 4 are not included in this article. The data for the charger is also included in Table 1 (Li et al., 2021; Tao et al., 2021).

## 3. Mathematical modeling

The microgrid considered comprises various DGs such as MT, FC, PV, WT, BESS, and the utility grid. Two objective functions are addressed: 1) operational cost minimization, and 2) emission minimization. An optimal EM process minimizes these objectives in single and multi-objective formulations, satisfying all constraints.

### 3.1. Objective Function

The two main objectives are discussed in the below section.

#### 3.1.1. Objective 1

The first objective aims to minimize the operational cost of the grid-connected microgrid through proper EM. Eq. (1) mathematically expresses this objective.

$$f1 = \text{Minimum\_Cost}_{(\text{Microgrid})} = \sum_{\tau=1}^T \text{Cost}(\tau) + OM_{\text{cost}} + OCPD_{\text{BESS}} \quad (4)$$

where,

$$\begin{aligned} \text{Cost}(\tau) = & \text{Cost}_G(\tau) + \text{Cost}_{DG}(\tau) + \text{Cost}_{BESS}(\tau) + \text{Startup\_Cost}_{fuel}(\tau) + \text{Startup\_Cost}_{MT}(\tau) \\ & + \text{Shutdown\_Cost}_{fuel}(\tau) + \text{Shutdown\_Cost}_{MT}(\tau) \end{aligned} \quad (5)$$

The power transfer between the utility grid and the microgrid can be defined in three ways, as described in 6-(8) (Bahmani-Firouzi & Azizipanah-Abarghooee, 2014; Sharma et al., 2016). In particular, the cost at which MG buys electricity from the utility is shown in 6, and the cost of the power that MG exports to the utility is expressed in 7. The MG's operating cost is zero if it neither buys nor sells any electricity to or from the utility, as shown by 8.

$$\text{Cost}_G(\tau) = \text{Bid}_G(\tau) \times W_G(\tau) \text{ if } W_G(\tau) > 0 \quad (6)$$

$$\text{Cost}_G(\tau) = (1 - \text{tax}) \text{Bid}_G(\tau) \times W_G(\tau) \text{ if } W_G(\tau) < 0 \quad (7)$$

$$\text{Cost}_G(\tau) = 0 \text{ if } W_G(\tau) = 0 \quad (8)$$

The total cost of power produced by all distribution-side resources is stated as (Bahmani-Firouzi & Azizipanah-Abarghooee, 2014; Sharma et al., 2016):

$$\begin{aligned} \text{Cost}_{DG}(\tau) = & (\text{Bid}_{fuel}(\tau) \times W_{fuel}(\tau) \times U_{fuel}(\tau)) + (\text{Bid}_{MT}(\tau) \times W_{MT}(\tau) \times U_{MT}(\tau)) + \\ & (\text{Bid}_{PV}(\tau) \times W_{PV}(\tau)) + (\text{Bid}_{WT}(\tau) \times W_{WT}(\tau)) \end{aligned} \quad (9)$$

The total cost of power related to the BESS is outlined below (Bahmani-Firouzi & Azizipanah-Abarghooee, 2014):

$$\text{Cost}_{BESS}(\tau) = (\text{Bid}_{BESS}(\tau) \times W_{BESS}(\tau) \times U_{BESS}(\tau)) \quad (10)$$

The startup costs for FC and MT are presented in Eqs. (11) and (12), respectively. Likewise, the shutdown costs for FC and MT are detailed in Eqs. (13) and (14) (Bahmani-Firouzi & Azizipanah-Abarghooee, 2014; Sharma et al., 2016). These costs pertain to both the current and past statuses.

$$\text{Startup\_Cost}_{fuel}(\tau) = \text{Start\_up}_{fuel} \times \max(0, U_{fuel}(\tau) - U_{fuel}(\tau - 1)) \quad (11)$$

$$\text{Startup\_Cost}_{MT}(\tau) = \text{Start\_up}_{MT} \times \max(0, U_{MT}(\tau) - U_{MT}(\tau - 1)) \quad (12)$$

$$\text{Shutdown\_Cost}_{fuel}(\tau) = \text{Shut\_down}_{fuel} \times \max(0, U_{fuel}(\tau - 1) - U_{fuel}(\tau)) \quad (13)$$

$$\text{Shutdown\_Cost}_{MT}(\tau) = \text{Shut\_down}_{MT} \times \max(0, U_{MT}(\tau - 1) - U_{MT}(\tau)) \quad (14)$$

The following is an expression of the entire cost of distributed

generation's operations and maintenance (Bahmani-Firouzi & Azizipanah-Abarghooee, 2014; Sharma et al., 2016):

$$OM_{\text{Cost}} = (OM_{\text{Cost}_{fuel}} + OM_{\text{Cost}_{MT}} + OM_{\text{Cost}_{PV}} + OM_{\text{Cost}_{WT}}) \times T \quad (15)$$

BESS is composed of individual battery units. There are two main costs associated with the BESS:  $F_C$  and  $MC$ . The expense of  $F_C$  is a singular cost involved in deploying and purchasing the battery units. The fixed cost is directly proportional to the battery size. Additionally,  $MC$ , measured in  $\text{€ct/kWh}$ , is an annual variable cost linked to the BESS size. The calculated value of  $MC$  is represented by  $\text{Size}_{BESS}(F_C + (l \times$

---

$MC_{BESS}))$ . The time constraint considered is one day, within which the total BESS cost is calculated. The illustration below shows the  $YAIIE$  for the BESS (Chen et al., 2011):

$$YAIIE = \frac{r(1+r)^l}{(1+r)^l - 1} F_C * \text{Size}_{BESS} \quad (16)$$

Here the lifetime of the BESS is denoted by  $l$ . ' $r$ ' represents the interest rate.  $\text{Size}_{BESS}$  indicates the battery size. One may get the overall cost of BESS by considering both the  $MC$  and the  $YAIIE$ . Finally, the mathematical expression for  $OCPD_{BESS}$  is given below (Bahmani-Firouzi & Azizipanah-Abarghooee, 2014; Chen et al., 2011).

$$OCPD_{BESS} = \frac{1}{365} [YAIIE + (\text{Size}_{BESS} \times MC)] \quad (17)$$

#### 3.1.2. Objective 2

The second goal is to reduce the net emissions of air pollutants from an MG's various DGs through proper EM. Specifically, the objective

---

function is linked to three of the most significant pollutants:  $\text{CO}_2$ ,  $\text{SO}_2$ , and  $\text{NO}_x$  (Aghajani & Ghadimi, 2018; Sedighizadeh et al., 2020).

$$f2 = \sum_{\tau=1}^T \text{Emission}(\tau) \quad (18) \quad \text{where, } \text{Emission}(\tau) = \text{Emission}_{MT}(\tau) + \text{Emission}_{FC}(\tau) + \text{Emission}_{BESS}(\tau) + \text{Emission}_{utility}(\tau) \quad (19)$$

All terms of (19) are explained in 20-(23) (Aghajani & Ghadimi, 2018; Sedighizadeh et al., 2020).

$$\text{Emission}_{MT}(\tau) = (U_{MT}(\tau) \times P_{MT}(\tau) \times E_{MT}(\tau)) \quad (20)$$

$$\text{Emission}_{FC}(\tau) = (U_{FC}(\tau) \times P_{FC}(\tau) \times E_{FC}(\tau)) \quad (21)$$

$$\text{Emission}_{BESS}(\tau) = (U_{BESS}(\tau) \times P_{BESS}(\tau) \times E_{BESS}(\tau)) \quad (22)$$

$$\text{Emission}_{Utility}(\tau) = (P_{utility}(\tau) \times E_{utility}(\tau)) \quad (23)$$

here,  $E_{MT}(\tau)$ ,  $E_{FC}(\tau)$ ,  $E_{BESS}(\tau)$ , and  $E_{utility}(\tau)$  are the pollutants' emission from MT, FC, BESS, and Utility, respectively, in kg/MWh (Aghajani & Ghadimi, 2018; Sedighizadeh et al., 2020). This article posits that emissions from utilities are always present, while emissions from FC, MT, and BESS depend on their operational status (starting up or shut-down). here,  $E_{MT}(\tau) = E_{MT\_CO2}(\tau) + E_{MT\_SO2}(\tau) + E_{MT\_NO}(\tau)$  (24)

The net  $\text{CO}_2$ ,  $\text{NO}_x$ , and  $\text{SO}_2$  emissions (kg/MWh) from the MT at a

particular time  $\tau$  are denoted as  $E_{MT\_CO2}(\tau)$ ,  $E_{MT\_NO}(\tau)$  and  $E_{MT\_SO2}(\tau)$  (Aghajani & Ghadimi, 2018; Sedighizadeh et al., 2020).

$$E_{FC}(\tau) = E_{FC\_CO2}(\tau) + E_{FC\_SO2}(\tau) + E_{FC\_NO}(\tau) \quad (25)$$

$E_{FC\_CO2}(\tau)$ ,  $E_{FC\_NO}(\tau)$  and  $E_{FC\_SO2}(\tau)$  indicate the amount of CO<sub>2</sub>, NO<sub>x</sub> and SO<sub>2</sub> emitted in kg/MWh from the FC at a given time  $\tau$  (Aghajani & Ghadimi, 2018; Sedighizadeh et al., 2020).

$$E_{BESS}(\tau) = E_{BESS\_CO2}(\tau) + E_{BESS\_SO2}(\tau) + E_{BESS\_NO}(\tau) \quad (26)$$

At any given moment, the values of  $E_{BESS\_CO2}(\tau)$ ,  $E_{BESS\_SO2}(\tau)$  and  $E_{BESS\_NO}(\tau)$  indicate the BESS's net CO<sub>2</sub>, SO<sub>2</sub>, and NO<sub>x</sub> emissions (kg/MWh), respectively (Aghajani & Ghadimi, 2018; Sedighizadeh et al., 2020).

$$E_{Utility}(\tau) = E_{Utility\_CO2}(\tau) + E_{Utility\_SO2}(\tau) + E_{Utility\_NO}(\tau) \quad (27)$$

The utility's emissions of CO<sub>2</sub>, SO<sub>2</sub>, and NO<sub>x</sub> are denoted by  $E_{Utility\_CO2}(\tau)$ ,  $E_{Utility\_SO2}(\tau)$ , and  $E_{Utility\_NO}(\tau)$ , respectively, and are measured in kg/MWh for a particular time period (Aghajani & Ghadimi, 2018; Sedighizadeh et al., 2020).

### 3.2. Constraints

There are various types of equality and inequality constraints necessary for the successful operation of the objective functions, as outlined below:

#### 3.2.1. Demand Equilibrium constraint

The total power generated through FC, PV, MT, and WT, as well as the received or supplied power from or to utility and battery, should be equal to the combination of the distribution side consumer demand ( $W_{Demand\_load}(\tau)$ ) and the PHEV charging load demand ( $W_{PHEV}(\tau)$ ) at the time  $\tau$  (Bahmani-Firouzi & Azizipanah-Abarghooee, 2014; Sharma et al., 2018).

$$W_{Demand\_load}(\tau) + W_{PHEV}(\tau) = (W_{fuel}(\tau) \times U_{fuel}(\tau)) + (W_{MT}(\tau) \times U_{MT}(\tau)) + W_{PV}(\tau) + W_{WT}(\tau) + (W_{BESS}(\tau) \times U_{BESS}(\tau)) + W_G(\tau) \quad (28)$$

#### 3.2.2. Active power constraint

The limits imposed on the operation of each DG unit are stated below (Aghajani & Ghadimi, 2018; Bahmani-Firouzi & Azizipanah-Abarghooee, 2014; Sedighizadeh et al., 2020; Sharma et al., 2018):

$$W_{fuel,min} \leq W_{fuel}(\tau) \leq W_{fuel,max} \quad \tau = 1, 2, 3, 4, \dots, T \quad (29)$$

$$W_{MT,min} \leq W_{MT}(\tau) \leq W_{MT,max} \quad \tau = 1, 2, 3, 4, \dots, T \quad (30)$$

$$W_{PV,min}(\tau) \leq W_{PV}(\tau) \leq W_{PV,max}(\tau) \quad \tau = 1, 2, 3, 4, \dots, T \quad (31)$$

$$W_{WT,min}(\tau) \leq W_{WT}(\tau) \leq W_{WT,max}(\tau) \quad \tau = 1, 2, 3, 4, \dots, T \quad (32)$$

#### 3.2.3. Energy Storage-Oriented constrain

The analysis in this work takes into account the advantages of lithium-ion battery over other BESS. These advantages include greater power concentration, lack of memory effects, and reduced charge loss while not in use (Bahmani-Firouzi & Azizipanah-Abarghooee, 2014; Sharma et al., 2018).

##### Discharging Mode:

The prevailing BESS discharge potential is entirely predicated on the

quantity of energy remaining in the system at the immediately preceding moment. After discharging the energy, the energy level of the battery must not fall below the BESS's minimum size. The BESS discharge mode is written as (Bahmani-Firouzi & Azizipanah-Abarghooee, 2014; Sharma et al., 2018):

$$\begin{aligned} E_{BESS}(\tau+1) &= \max \left\{ \left( E_{BESS}(\tau) - \frac{\Delta \tau \times W_{BESS}(\tau)}{\eta_d} \right), E_{BESS,min} \right\} \quad \tau \\ &= 1, 2, 3, 4, \dots, T \end{aligned} \quad (33)$$

$$W_{charge\_rate_{BESS}}(\tau) \leq W_{BESS}(\tau) \leq W_{discharge\_rate_{BESS}}(\tau) \quad (34)$$

##### Charging Mode:

The BESS charging phenomena is determined at every instance by the energy that has gathered from the preceding instant. The amount of energy storage ability in the BESS must be limited to its maximal capacity (Bahmani-Firouzi & Azizipanah-Abarghooee, 2014; Sharma et al., 2018).

$$\begin{aligned} E_{BESS}(\tau) &= \min \left\{ (E_{BESS}(\tau) - (\Delta \tau \times W_{BESS}(\tau) \times \eta_c)), E_{BESS,max} \right\} \quad \tau \\ &= 1, 2, 3, 4, \dots, T \end{aligned} \quad (35)$$

$$W_{charge\_rate_{BESS}}(\tau) \leq W_{BESS}(\tau) \leq W_{discharge\_rate_{BESS}}(\tau) \quad (36)$$

where,

$$\begin{aligned} W_{discharge\_rate_{BESS}}(\tau) &= \min \left\{ W_{BESS,max}, \frac{(E_{BESS}(\tau) - E_{BESS,min}) \times \eta_c}{\Delta \tau} \right\} \quad \tau \\ &= 1, 2, 3, 4, \dots, T \end{aligned} \quad (37)$$

$$\begin{aligned} W_{charge\_rate_{BESS}}(\tau) &= \max \left\{ W_{BESS,min}, \frac{(E_{BESS}(\tau) - E_{BESS,max})}{(\eta_c \times \Delta \tau)} \right\} \quad \tau \\ &= 1, 2, 3, 4, \dots, T \end{aligned} \quad (38)$$

#### 3.2.4. Grid Constraints

The utility's power generation is restricted by both an upper and a lower bound within every time period (Bahmani-Firouzi & Azizipanah-Abarghooee, 2014; Sharma et al., 2018).

$$W_{grid,min} \leq W_G(\tau) \leq W_{grid,max} \quad \tau = 1, 2, 3, 4, \dots, T \quad (39)$$

### 4. SMA implementation in the Mg test system

SMA is a widely adopted population-based metaheuristic technique that emphasizes inducing morphological and behavioral changes instead of representing the slime mould's complete growth stages (Li et al., 2020). SMA is applied in this study because of its high efficacy, fast convergence rate and easy set-up in resolving nonlinear functions and ease of implementation.

#### 4.1. SMA modeling

The following three processes are involved in SMA modeling:

##### 4.1.1. Approach Food

The slime mould is modeled using the following formula, which mimics contraction mode (Liang et al., 2021).

$$P(t+1) = P_b(t) + \theta_b(G \times P_A(t) - P_B(t)) \quad r < s \quad (40)$$

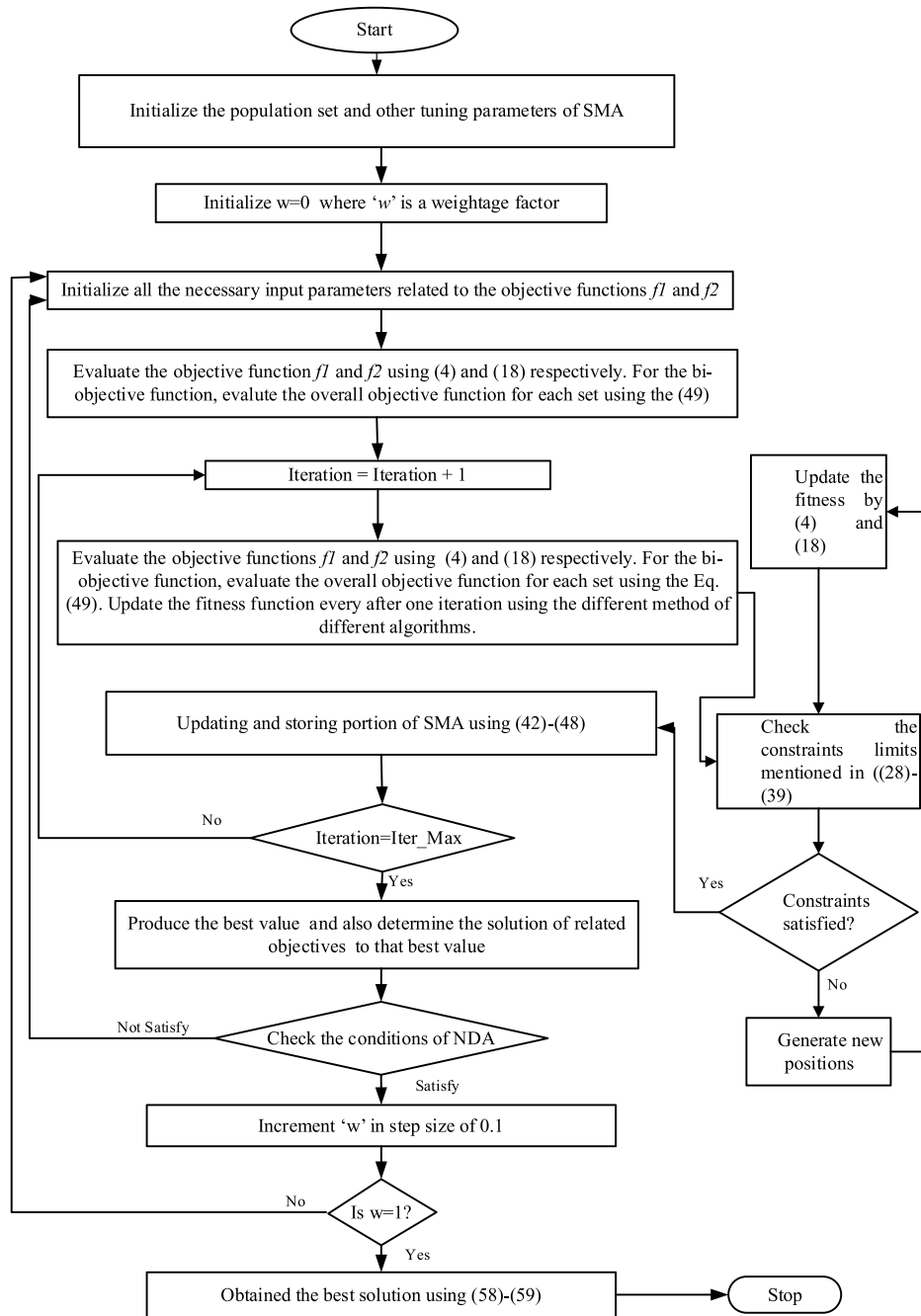


**Fig. 2.** Flowchart of multi-objective solution approach for objectives 1 and 2.

$$= \theta_c \times P(t)r > s \quad (41)$$

' $\theta_b$ ' has a range of  $[-a, a]$ , whereas ' $\theta_c$ ' progressively decreases to zero.  $P_b$  represents the individual regions that currently exhibit the highest concentrations of available emissions, and 't' stands for the most recent iteration.  $P(t)$  denotes the slime mould's position.  $P_A$  and  $P_B$  indicate for two random members of the swarm, and  $G$  stands for the slime mould's weight. An expression for 's' is as follows (Li et al., 2020):

$$s = \tanh|Y(k) - FF| \quad k = 1, 2, \dots, n \quad (42)$$

$Y(k)$  is a representation of  $P$ 's fitness.  $FF$  stands for the optimal fitness function over all iterations.  $\theta_b$  and  $\theta_c$  have the following formulas (Li et al., 2020):

$$\theta_b = [-a, a] \quad (43)$$

$$\text{here, } a = \text{arctanh} \left( - \left( \frac{t}{\max\_t} \right) + 1 \right) \quad (44)$$

$$\theta_c = [-b, b] \quad (45)$$

$$\text{here, } b = \left( 1 - \frac{t}{\max\_t} \right) \quad (46)$$

The following is the expression for  $G$ :

$$G(S\_Index(k)) = 1 + r \log \left( \frac{b_f - Y(k)}{b_f - w_f} + 1 \right), \text{ condition} \quad (47)$$

$$= 1 - r \log \left( \frac{b_f - Y(k)}{b_f - w_f} + 1 \right), \text{ other}$$

$$S\_Index = \text{sort}(Y) \quad (48)$$

According to 'conditions,'  $Y(k)$  rank is in the upper half of the population. The symbol 'r' denotes a freely selectable integer between 0 and 1.  $w_f$  and  $b_f$  represent the worst optimal solution and the best fitness value, respectively, in the current iterations. The series of sorting values for fitness (which ascends in the minimal value problem) is shown by 'S\_Index'.

#### 4.1.2. Wrap Food

This part provides a mathematical description of how the venous tissue of the slime mold contracts in search of sustenance. The modified location of the slime mold is stated as follows (S. Li et al., 2020):

$$P = \text{rand}(UU - LL) + LL \quad \text{rand} < z \quad (49)$$

$$P_b(t) + \theta_b \cdot (G.P_A(t) - P_B(t)) \quad r < s \quad (50)$$

$$= \theta_c \cdot P(t) \quad r \geq s \quad (51)$$

The search range of lower and upper boundaries is denoted by the  $LL$  and  $UU$ . Two arbitrary integers 'rand' and 'r' lies in the interval [0, (Katiraei et al., 2008)].

#### 4.1.3. Oscillation

As the number of iterations increases, the variable ' $\theta_b$ ' gradually slants zero and before that it fluctuates freely within the range [-a, a]. Meanwhile, the variable  $\theta_c$  oscillates within the interval [-1, 1] until it finally settles at zero.

### 5. Multi-objective solution approach

This work employs the weighted sum approach, fuzzy decision methodology, and several metaheuristic algorithms (SMA, GOA, SCA) to solve the multi-objective economic-emission dispatch problem, while maintaining non-dominated solutions.

#### 5.1. Weighted Sum method

WSM is used to create a single objective by combining many objective functions. This is done by giving weights to each objective based on their relative importance. The combined objective function, represented by 52, incorporates the linearity factor  $\zeta$  (€ct/kg) to account for the varying ranges of value of the individual objectives (Aghajani & Ghadimi, 2018; Chakraborty & Ray, 2024).

$$f = w \times f_1 + (1-w) \times \zeta \times f_2 \quad (52)$$

'w' represents the assigned weighted value for one objective, while  $(1-w)$  is the weighting of the other objective. The weighting factor step size in this study is fixed at 0.1. The explanation of the factor  $\zeta$  is as follows:

$$\zeta = \frac{f_1^{\max}(t)}{f_2^{\max}(t)} \quad (53)$$

$f_1^{\max}(t)$  and  $f_2^{\max}(t)$  denote the greatest figures of  $f_1$  and  $f_2$ , respectively, within the population set for a given iteration.

#### 5.2. Non-dominated approach

The overall framework for a multiple-objective issue defined by both equational and inequational conditions is outlined in 54.

$$\min_{s.t.t \in X} Y = (f_1(N), f_2(N), f_3(N), \dots, f_n(N))^T = F(N) \quad (54)$$

Here,  $N$  is an n-dimensional vector representing the choice variables,  $X$  is the decision space, and  $n$  is the total number of objective functions. Now,  $N_i$  is considered to be dominated by  $N_j$ , shown as  $N_i \prec N_j$  (Chakraborty & Ray, 2024).

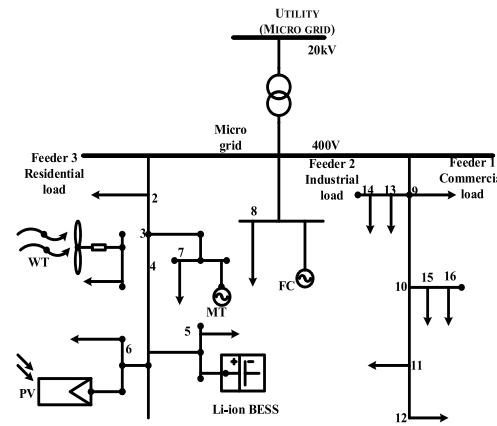


Fig. 3. MG test system.

Table 2

Considered data limits of various generating and storage units.

Type	WT	PV	MT	FC	BESS	Utility
Highest power (kW)	15	25	30	30	30	30
Lowest power (kW)	0	0	6	3	-30	-30
Startup/Shutdown Cost (€ct)	-	-	0.96	1.65	-	-
Bid (€ct/kWh)	1.073	2.584	0.457	0.294	0.38	-

Table 3

Emission co-efficient of different DGs.

Source	CO <sub>2</sub> (kg/MWh)	NO <sub>x</sub> (kg/MWh)	SO <sub>2</sub> (kg/MWh)
FC	460	0.0075	0.003
MT	720	0.1	0.0036
PV	0	0	0
WT	0	0	0
BESS	10	0.001	0.0002
Utility	950	2.1	0.5

$$f_x(N_i) \leq f_x(N_j), \quad \forall x \in \{1, 2, \dots, X\} \quad (55)$$

$$f_x(N_i) < f_x(N_j), \quad \exists x \in \{1, 2, \dots, X\} \quad (56)$$

The two responses,  $N_i$  and  $N_j$ , are stated to be non-dominated, with the condition that neither  $N_i \prec N_j$  nor  $N_j \prec N_i$ .

The objective function  $F$  takes the form of a multi-dimensional vector, treating the two objectives equitably, without favoring one over the other. This vector-based objective  $F$ , as stated in (57), is the target of the optimization strategy known as the NDA. The main goal of the NDA is to identify a dispatch that minimizes the objective while satisfying the constraints associated with vector  $F$  (Chakraborty & Ray, 2024).

$$F = (f_1, f_2) \quad (57)$$

Employing a fuzzy decision-maker method the best Pareto optimum outcome from the Pareto front is determined.

#### 5.3. Fuzzy decision maker approach

In a multi-objective problem, every objective function is given a weightage value 'w' between 0 and 1, with the aim of making sure that the sum of all weighting factors equals to 1. The process is then run again, increasing the weighting factor by a constant step size as it goes from 0 to 1. This method yields a non-dominated set of solutions known as the Pareto optimum solutions and this fuzzy approach selects the best set from the Pareto front. The following membership function is presented to facilitate the reduction of the objective functions:

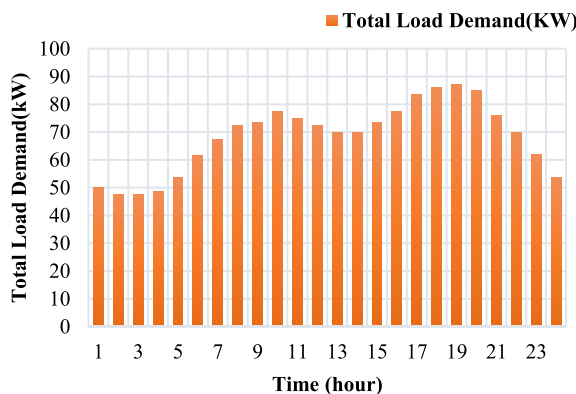


Fig. 4. Forecasted load demand for a day.

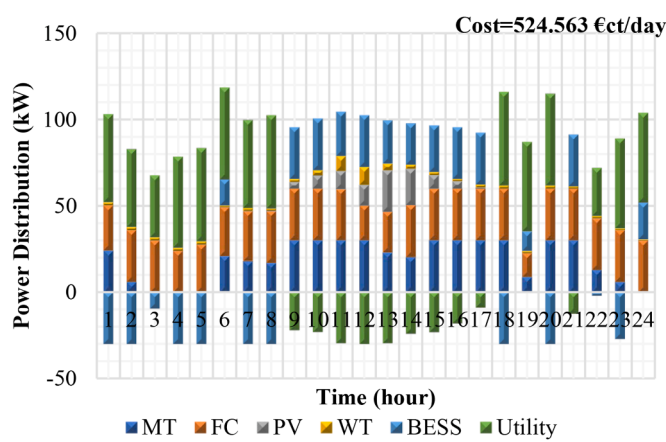


Fig. 5. Smart charging technique-based power distribution of different DGs for minimum operating cost using SMA (Scenario-I).

$$u_{j_i} = \begin{cases} 1 & \text{if } F_i \leq F_i^{\min} \\ \frac{F_i^{\max} - F_i}{F_i^{\max} - F_i^{\min}} & \text{if } F_i^{\min} < F_i < F_i^{\max} \\ 0 & \text{if } F_i \geq F_i^{\max} \end{cases} \quad (58)$$

When (59) reaches its peak value, the optimal non-dominated objective function is determined, as the largest magnitude of the normalized summation of the values of all the objective functions.

$$\mu^k = \frac{\sum_{i=1}^Q \mu_{j_i}^k}{\sum_{k=1}^M \sum_{i=1}^Q \mu_{j_i}^k} \quad (59)$$

"Q" is a representation of the total number of objective functions. In this research paper, "Q" is set to 2. "M" represents the quantity of non-dominated solutions. Upon completion of the procedure, the most effective solution to the issue is determined. Fig. 2 illustrates the various steps of SMA used to find the EM of an MG using a multi-objective function (Chakraborty & Ray, 2024; Sedighizadeh et al., 2020; Zandrazavi et al., 2022).

## 6. Result and discussion

This study examines a low-voltage microgrid test system, and Fig. 3 presents its single-line diagram, which shows the utility grid connected to the microgrid test system via a transformer (Bahmani-Firooz & Azizipanah-Abarghooee, 2014; Sharma et al., 2018).

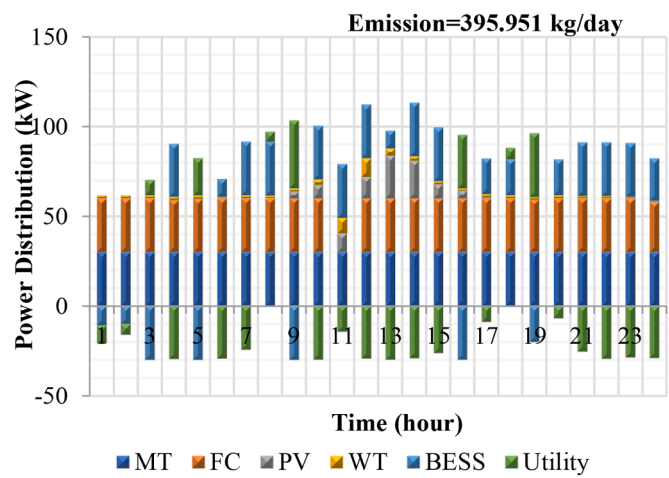


Fig. 6. Smart charging technique-based power distribution of different DGs for minimum net pollution emissions applying SMA (Scenario-I).

Table 4

Smart charging technique based operating cost (€ct/day) over multiple simulation runs: Scenario-I.

Applied algorithm	Best outcome	Mean outcome	Worst outcome	Hits of achieving the best outcome
SCA	595.285	595.29	595.321	26
GOA	554.163	554.165	554.184	27
SMA	524.563	524.564	524.601	29

Table 5

Smart charging technique based net pollution emission (kg/day) over multiple simulation runs: Scenario-I.

Applied algorithm	Best outcome	Mean outcome	Worst outcome	Hits of achieving the best outcome
SCA	425.018	425.044	425.213	26
GOA	417.318	417.321	417.345	27
SMA	395.951	395.953	395.998	29

### 6.1. Microgrid Test system

In this research article, an MG is designed with different DGs (like FC, MT, PV, and WT) along with BESS as a storage system. The bid prices (€ct/kWh), startup and shutdown costs (€ct/kWh), maximum and minimum power limitations (kW), and operation and maintenance cost

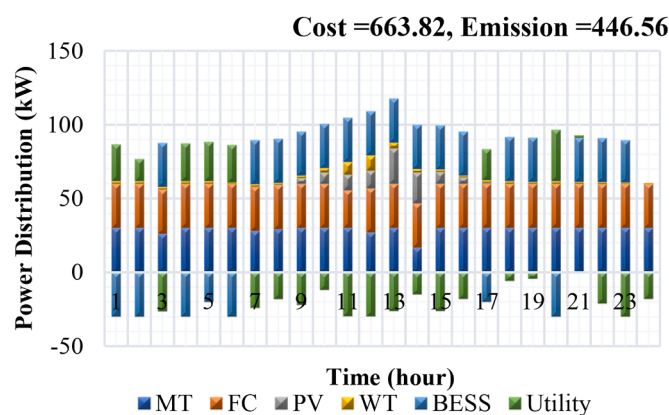


Fig. 7. Smart charging technique-based power distribution of various DGs for minimum operational costs and pollution emissions through a multi-objective function using SMA (Scenario-I).

**Table 6**

Optimum results for a multi-objective function (Scenario-I).

Applied algorithm	Objective Function	
	Operational Cost (€ct/day)	Emission(kg/day)
SCA	742.143	488.102
GOA	692.751	482.304
SMA	663.828	446.561

coefficients (€ct/kWh) of various generating units and BESS are mentioned in Table 2 (Bahmani-Firouzi & Azizipanah-Abarghooee, 2014; Sharma et al., 2018). Pollution emission coefficients (kg/MWh) of various pollutants are mentioned in Table 3 (Aghajani & Ghadimi, 2018; Sedighizadeh et al., 2020). The 24-hour forecasted power output for PV and WT systems has been derived from the refs (Bahmani-Firouzi & Azizipanah-Abarghooee, 2014; Chakraborty & Ray, 2024; Sharma et al., 2018). Additionally, the utility's real-time market energy prices during the same moment have also been obtained from these sources. Fig. 4 presents the predicted total load demand for a given day (Bahmani-Firouzi & Azizipanah-Abarghooee, 2014; Kumar & Karthikeyan, 2024). This study assumes that DGs can only supply active power with a power factor of unity. The BESS can hold 500 kWh at its greatest capacity and 50 kWh at its least. This indicates that the battery's permitted capacity range is [50–500]. A 10 % tax is taken into account. Hourly assessments are made throughout the day (Bahmani-Firouzi & Azizipanah-Abarghooee, 2014; Sharma et al., 2018).

This article considers level 1 and level 2 charging patterns. The values of  $\sigma_{PHEV}^{\min}$  and  $\sigma_{PHEV}^{\max}$  are kept at 0–50 kW for house hold locations and 5–70 kW for public locations during the smart charging process. Throughout the day, a total of 70 PHEVs charge themselves either partially or fully according to their needs. When load constraints are taken into account, (28) states that the generated power must equal the sum of consumer load ( $W_{Demand\_load,t}$ ) and PHEV charging load ( $W_{PHEV,t}$ ).

Now the determination of  $W_{PHEV,t}$  depends on the  $\left(\frac{\theta_m(\tau)}{\gamma_{PHEV}} \times \sigma_{PHEV}(\tau)\right)$ . By

smartly optimizing the term  $\left(\frac{\theta_m(\tau)}{\gamma_{PHEV}} \times \sigma_{PHEV}(\tau)\right)$ , it can effectively distribute the impact of PHEV charging over the day, ultimately helping to reduce operational cost and emissions in the MG. This study examines three scenarios that occur during an MG's EM. In Scenario-I, the BESS is initially charged to zero, and all of the DGs are in a startup/ shutdown (or on/off) state. In Scenario-II, BESS is initially charged to its maximum state-of-charge and all DGs remain in the startup/shutdown (or on/off) phase based on economic preference. In Scenario-III, the BESS holds the highest energy at the initial moment, and all DGs are kept in the startup (or "on") state. All three scenarios are controlled by the smart charging technique. SMA is used in all scenarios to figure out the best EM for the MG and compare its results to those of other algorithms, such as SCA and GOA. The solution approach is developed on MATLAB 2016b platform of a personal computer with 8 GB RAM and an Intel i3 CPU.

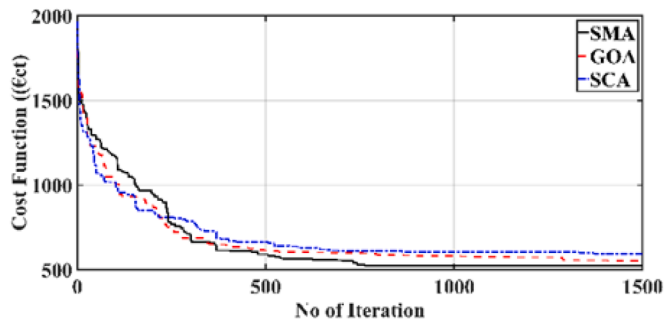


Fig. 8. Convergence curve of different algorithm for minimum operating cost (Scenario-I).

#### 6.1.1. Scenario-I

In Scenario-I, the MG is equipped with a BESS that starts with no initial charge. Based on economic considerations, DGs are either in startup or shutdown states. As the Li-ion battery begins with no charge,

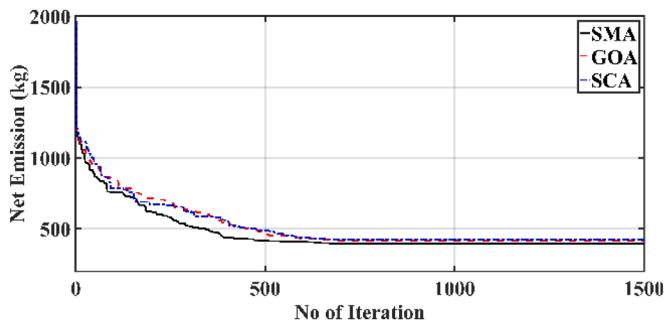


Fig. 9. Convergence curve of different algorithm for minimum pollution emission (Scenario-I).

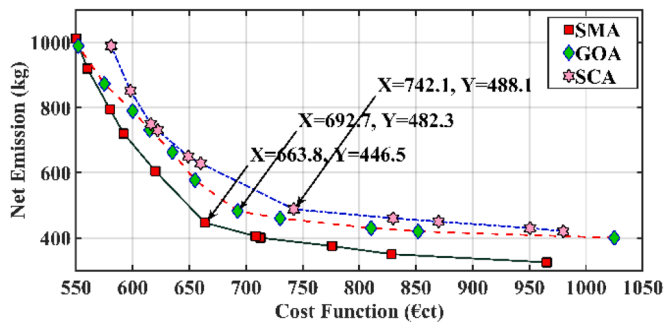


Fig. 10. Pareto-Optimal front for Scenario-I.

**Table 7**

Fuzzy clustering step along with SMA to address the multi-objective issue for Scenario-I.

Sequence number	w	(1-w)	f1	f2	f1 <sub>pu</sub>	f2 <sub>pu</sub>	Min (f1 <sub>pu</sub> , f2 <sub>pu</sub> )
1	0	1	965.3	325	0	1	0.069832402
2	0.1	0.9	828.4	350	0.329641223	0.963609898	0.090310832
3	0.2	0.8	775.9	375	0.456055863	0.927219796	0.096597462
4	0.3	0.7	712.8	400	0.607994221	0.890829694	0.104666475
5	0.4	0.6	708.5	405	0.618348182	0.883551674	0.104881275
6	0.5	0.5	663.8	446.5	0.725981218	0.823144105	0.108179143
7	0.6	0.4	620	605	0.831447147	0.592430859	0.099432822
8	0.7	0.3	592	720.7	0.898868288	0.424017467	0.09238029
9	0.8	0.2	580	794.6	0.927763063	0.316448326	0.08688627
10	0.9	0.1	560	919.7	0.975921021	0.134352256	0.07753305
11	1	0	550	1012	1	0	0.069832402

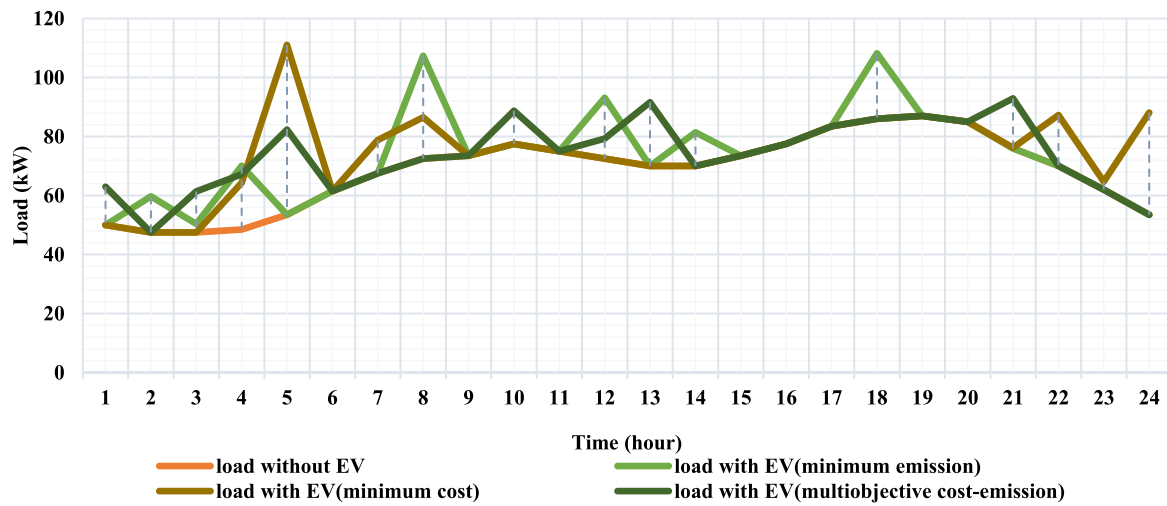


Fig. 11. Loading effect analysis for Scenario-I.

Table 8

Smart charging technique based total operating cost (€ct/day) over multiple simulation runs: Scenario-II.

Applied algorithm	Best outcome	Mean outcome	Worst outcome	Hits of achieving the best outcome
SCA	409.7744	409.777	409.8012	26
GOA	407.1992	407.2073	407.3211	28
SMA	405.5322	405.5342	405.5932	29

Table 9

Smart charging technique based net emission(kg/day) over multiple simulation runs: Scenario-II.

Applied algorithm	Best outcome	Mean outcome	Worst outcome	Hits of achieving the best outcome
SCA	428.423	428.426	428.461	27
GOA	415.029	415.04	415.1451	27
SMA	413.896	413.899	413.921	29

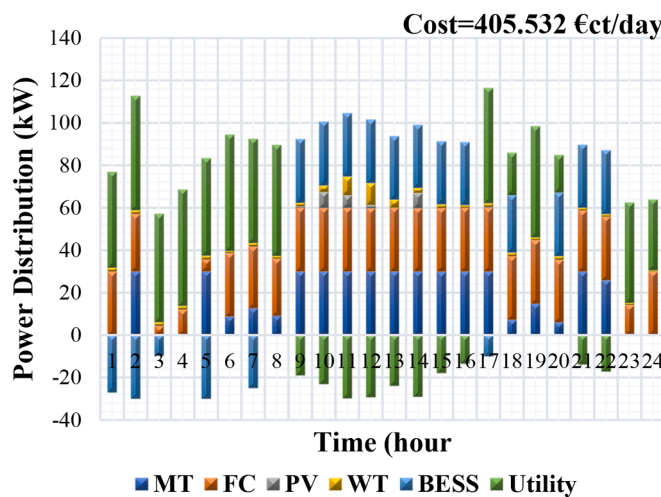


Fig. 12. Smart charging technique-based power distribution of different DGs for minimum operating cost using SMA (Scenario-II).

the discharge power of the BESS is determined by the energy accumulated in the preceding hours. The power distribution using SMA for this scenario is depicted in Figs. 5 and 6, to demonstrate the lowest possible

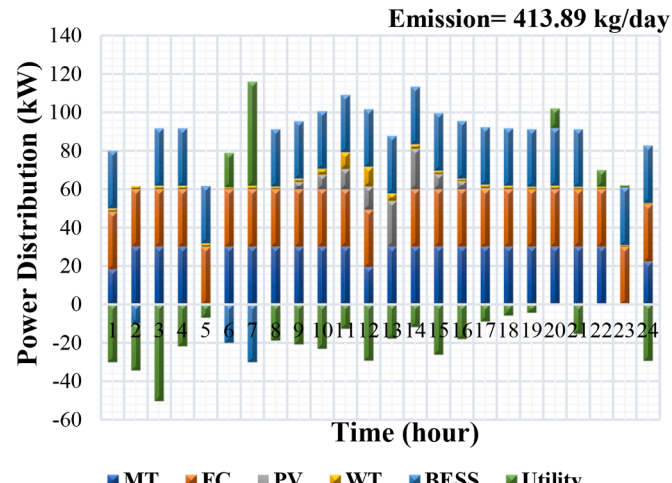


Fig. 13. Smart charging technique-based power distribution of different DGs for minimum net pollution emissions using SMA (Scenario-II).

Table 10

Optimum results for a multi-objective function (Scenario-II).

Applied algorithm	Objective Function	
	Operational Cost (€ct/day)	Emission(kg/day)
SCA	677.7	520.2
GOA	531.6	669.6
SMA	538.6	529.8

operating cost and emission, respectively. As indicated in Table 4, the least operation cost utilizing SMA is 524.563 €ct/day, and the result is contrasted with various optimization methods. In comparison to GOA and SCA, Table 5 shows that the minimal pollution from an MG utilizing SMA is 395.951 kg/day. Figs. 5 and 6 show, respectively, that pollution emissions rise too high to attain the lowest possible cost, while at the same time, extreme costs are required to achieve the lowest possible net emissions. This work adopts a multi-faceted solution methodology that identifies Pareto-optimal solutions, aiming to minimize both the economic expenses and environmental emissions to tackle this challenge. Fig. 7 illustrates how to distribute the power of different generating units using SMA to meet load demand while achieving the optimal cost and emission levels at the same time. According to the Pareto-optimal

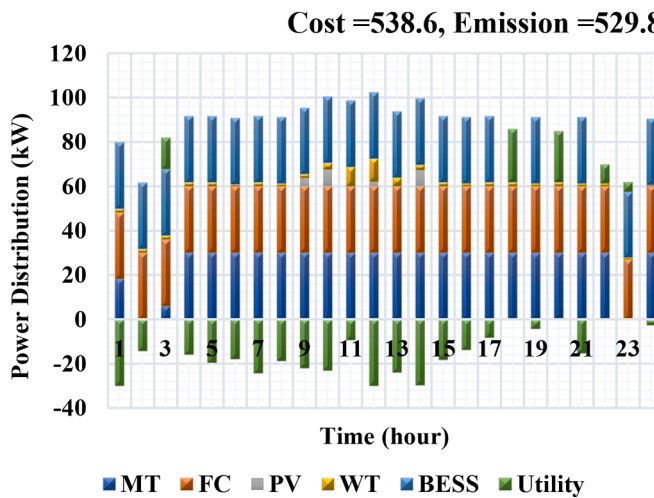


Fig. 14. Smart charging technique-based power distribution of various DGs for minimum operational costs and pollution emissions through a multi-objective function using SMA (Scenario-II).

front, the best possible set of costs and net emissions using SMA is 663.828 €ct/day and 446.561 kg/day. SMA, GOA, and SCA results for the multi-objective function in Scenario-I are displayed in Table 6. Table 7 shows the multi-objective approach's last phase, which SMA created with a step size of 0.1. The comparative analysis of load control by SMA for Scenario-I is shown in Fig. 11. Without PHEV, the base load is interpreted as a load arising from the consumer's side in this instance. A close examination of Fig. 11 reveals that the majority of PHEV charging demand is met during off-peak periods by the energy management of the multi-objective function. Figs. 8 and 9 display the convergence graphs for SMA, SCA, and GOA in estimating optimal cost and emissions, while Fig. 10 presents the Pareto-optimal trade-off curve between cost and emissions for Scenario-I using these optimization algorithms.

#### 6.1.2. Scenario-II

In this scenario, the Li-Ion BESS is assumed to begin with a charge level close to full capacity, while the DGs are managed based on economic considerations. As illustrated in Table 8, the lowest daily operating cost achieved using SMA is 405.5322 €ct/day, outperforming other optimization methods. Minimum pollution emissions of the MG in this scenario during load management using different algorithms are illustrated in Table 9. Figs. 12 and 13 illustrate the optimal power management for Scenario-II using SMA, which achieves the lowest operational cost and the least net emissions, respectively. These figures demonstrate that cost minimization results in higher pollution emissions, while achieving the lowest net pollution emissions entails a significant operational cost. The proposed approach utilizes a multi-objective function based on the Pareto-optimal set to concurrently

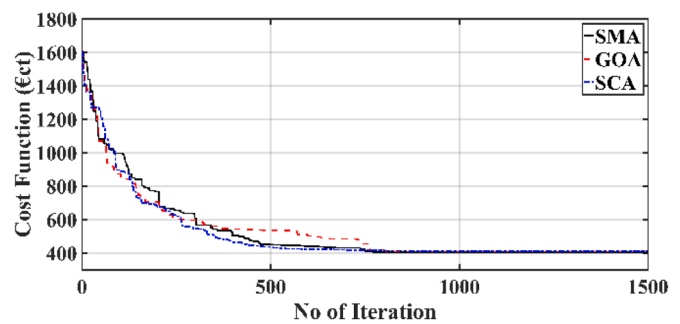


Fig. 15. Convergence curve of different algorithm for minimum operating cost (Scenario-II).

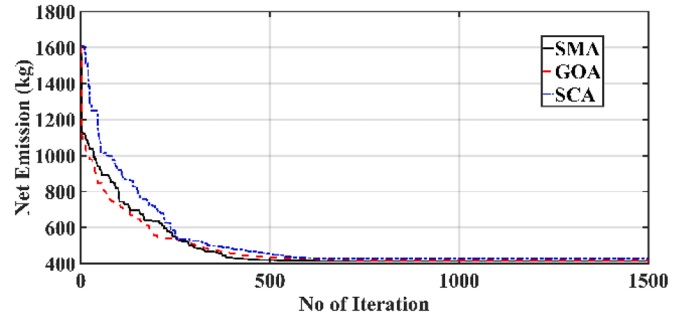


Fig. 16. Convergence curve of different algorithm for minimum net emission (Scenario-II).

minimize both the operating cost and net emissions. The Pareto-optimal set in Scenario-II, obtained through SMA combined with WSM and the fuzzy decision-maker, yields operating cost and emission values of 538.6 €ct/day and 529.8 kg/day, respectively. Table 10 summarizes the outcomes of the multi-objective function for SMA, SCA, and GOA. Fig. 14 depicts the power profile related to the Pareto-optimal front for Scenario-II, while Table 11 details the use of the fuzzy decision maker

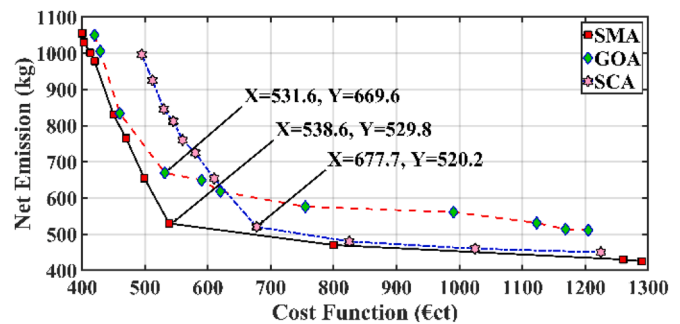


Fig. 17. Pareto-Optimal front for Scenario-II.

Table 11

Fuzzy clustering step along with SMA to address the multi-objective issue for Scenario-II.

Sequence number	w	(1-w)	f1	f2	f1 <sub>pu</sub>	f2 <sub>pu</sub>	Min (f1 <sub>pu</sub> , f2 <sub>pu</sub> )
1	0	1	1290	425	0	1	0.0735186
2	0.1	0.9	1260	430	0.033707865	0.99207607	0.075414199
3	0.2	0.8	800	470	0.550561798	0.928684628	0.108752127
4	0.3	0.7	<b>538.6</b>	<b>529.8</b>	<b>0.844269663</b>	<b>0.833914422</b>	<b>0.123377745</b>
5	0.4	0.6	499	655	0.888764045	0.635499208	0.112061701
6	0.5	0.5	470	765	0.921348315	0.461172742	0.101641013
7	0.6	0.4	450	830.5	0.943820225	0.357369255	0.095661629
8	0.7	0.3	420	978	0.97752809	0.123613312	0.080954375
9	0.8	0.2	413	1001	0.985393258	0.087163233	0.078852852
10	0.9	0.1	403	1030	0.996629213	0.041204437	0.076300077
11	1	0	400	1056	1	0	0.0735186

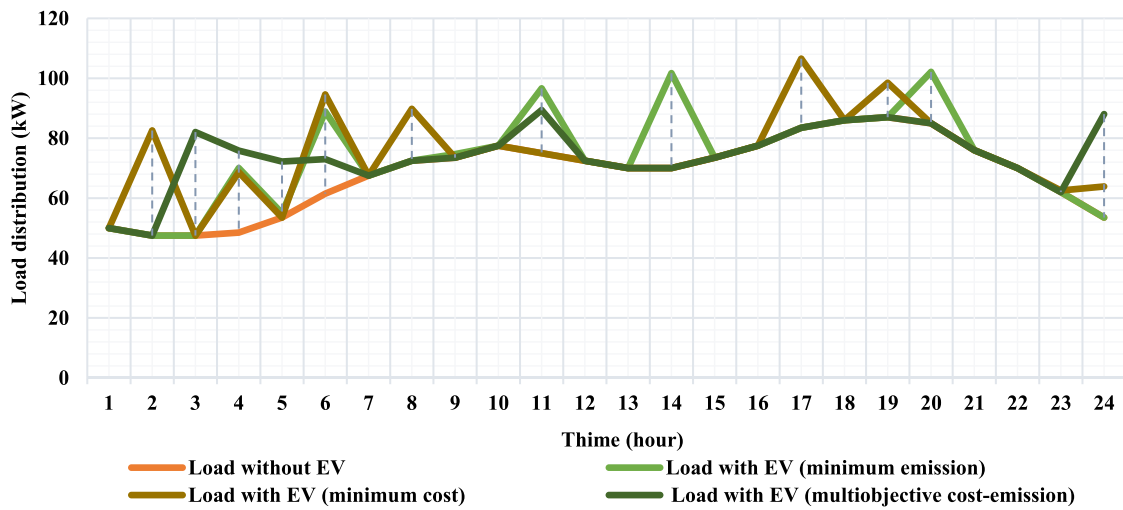


Fig. 18. Loading effect analysis for Scenario-II.

Table 12

Smart charging technique based on total operating cost (€ct/day) over multiple simulation runs: Scenario-III.

Applied algorithm	Best outcome	Mean outcome	Worst outcome	Hits of achieving the best outcome
SCA	534.8698	534.8729	534.9012	27
GOA	524.2765	524.2801	524.3125	27
SMA	514.8745	514.8753	514.8986	29

Table 13

Smart charging technique based net emission (kg/day) over multiple simulation runs: Scenario-III.

Applied algorithm	Best outcome	Mean outcome	Worst outcome	Hits of achieving the best outcome
SCA	358.12	358.124	358.16	27
GOA	356.82	356.823	356.87	28
SMA	352.74	352.7403	352.749	29

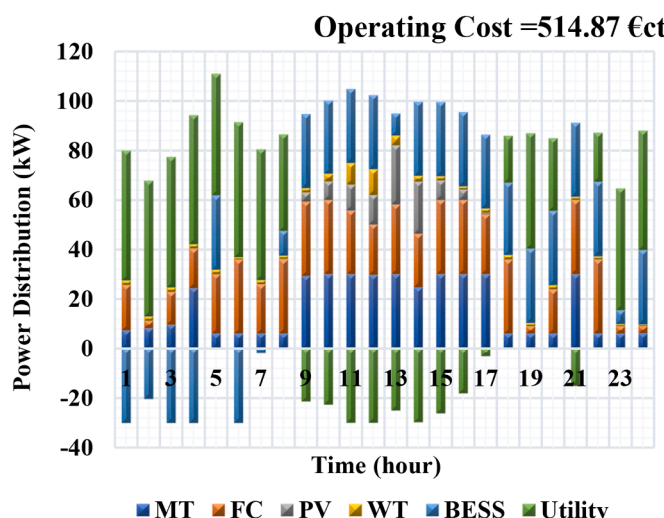


Fig. 19. Smart charging technique-based power distribution of different DGs for minimum operating cost using SMA (Scenario-III).

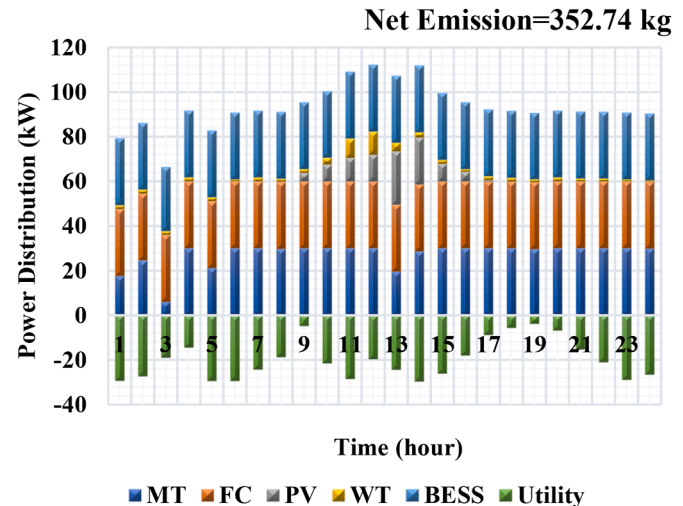


Fig. 20. Smart charging technique-based power distribution of different DGs for minimum net pollution emissions using SMA (Scenario-III).

concept in the multi-objective approach, executed using SMA with a step increment of 0.1. Fig. 18 depicts the comparative assessment of load control for different processes performed by SMA in Scenario-II. Analysis of Fig. 18 demonstrates how the extra load from PHEV charging is met in various situations, and it is clear that the multi-objective function-based EM satisfies nearly all PHEV charging demands during off-peak hours. The convergence graphs of SMA, SCA and GOA to calculate the minimal cost and emission, respectively, are drawn in Figs. 15 and 16. Fig. 17 depicts the Pareto-optimal front graphs for Scenario-II using SCA, GOA, and SMA.

#### 6.1.3. Scenario-III

In Scenario-III, the lithium-ion battery's initial charge is assumed to equal the battery's maximum capacity. All the generating units, including the storage system, are always kept in startup mode. Tables 12 and 13 provide the outcomes of SMA and other methods for the least operating cost and pollutant emission of an MG, respectively. The optimal power divisions among the DGs, storage system and main grid, to get the lowest possible operating cost and emission, respectively, for Scenario-III using SMA are shown in Figs. 19 and 20. The outcomes of the Pareto front for cost and pollution emission using different algorithms are shown in Table 14. Fig. 21 shows the power utilization of

**Table 14**

Optimum results for a multi-objective function (Scenario-III).

Applied algorithm	Objective Function	
	Operational Cost (€ct/day)	Emission(kg/day)
SCA	781.9	424.1
GOA	768.2	411.5
SMA	712.6	385.9

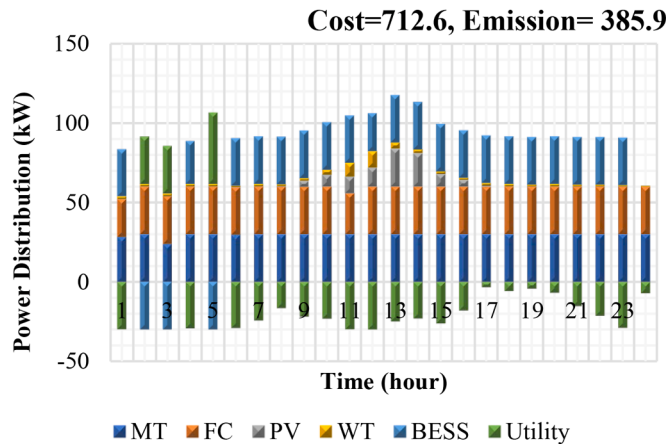


**Fig. 21.** Smart charging technique-based power distribution of various DGs for minimum operational costs and pollution emissions through a multi-objective function using SMA (Scenario-III).

various generating units during the Pareto-optimal solution using SMA method, which yields an operational cost of 712.6 €ct/day and emission of 385.9 kg/day. Table 15 shows the final step of the multi-objective approach with a step size of 0.1 developed by SMA. Loading effect analysis to emphasize the efficacy of multi-objective function-based EM during load mitigation of PHEV charging is shown in Fig. 25. Convergence graphs of different algorithms for Scenario-III to achieve minimal cost and emission, respectively, are shown in Figs. 22 and 23. The Pareto-optimal front-based SMA, GOA, and SCA graphs for this scenario are shown in Fig. 24.

## 6.2. Comparative analysis and discussion

Comparisons of the minimum operating cost obtained using SMA, SCA and GOA for three scenarios are indicated in Tables 4, 8, and 12, respectively. Similarly, comparisons between SMA, GOA, and SCA in achieving the lowest possible net emissions of pollutants for Scenarios I, II, and III are presented in Tables 5, 9, and 13, respectively. This paper also presented a multi-objective function-based Pareto-optimal solution using three algorithms, and the results are compared in Tables 6, 10, and

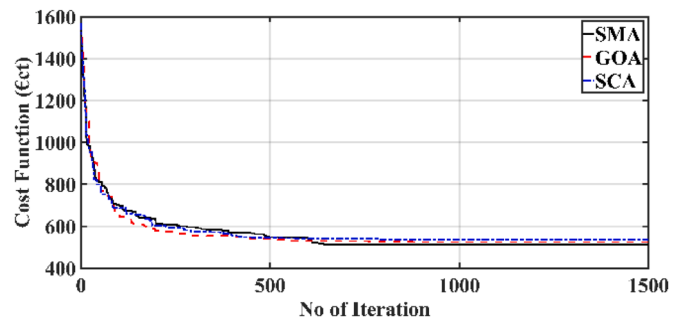


**Fig. 22.** Convergence curve of different algorithm for minimum operating cost (Scenario-III).

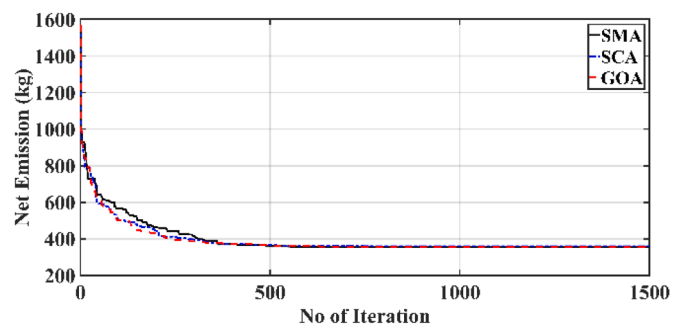


**Fig. 23.** Convergence curve of different algorithm for minimum net emission (Scenario-III).

14 for Scenarios I, II, and III, respectively. The primary objective here is to demonstrate how a multi-objective function-driven EM process facilitates the simultaneous reduction of costs and emissions. This is crucial because the other two EM approaches employed across the three scenarios exhibit an inverse relationship - when one process minimizes operational costs, the resulting pollution emissions become excessively

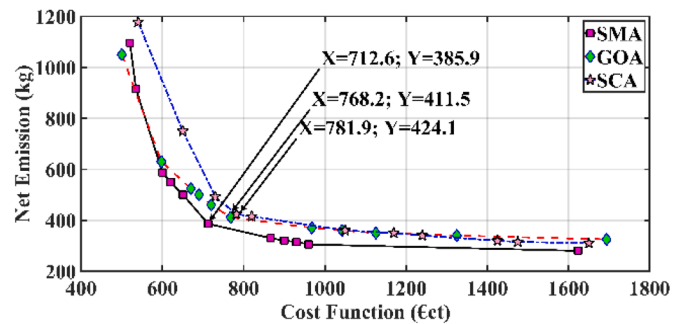


**Fig. 24.** Pareto-Optimal front for Scenario-III.

**Table 15**

Fuzzy clustering step along with SMA to address the multi-objective issue for Scenario-III.

Sequence number	w	(1-w)	f1	f2	f1 <sub>pu</sub>	f2 <sub>pu</sub>	Min (f1 <sub>pu</sub> , f2 <sub>pu</sub> )
1	0	1	1624	280	0	1	0.062378207
2	0.1	0.9	960	305	0.60144928	0.96932515	0.097982092
3	0.2	0.8	930	315	0.62862319	0.95705521	0.098911775
4	0.3	0.7	900	320	0.6557971	0.95092025	0.100224147
5	0.4	0.6	866.3	330	0.68632246	0.93865031	0.101362887
6	0.5	0.5	712.6	385.9	0.82554348	0.87006135	0.105768788
7	0.6	0.4	650.5	500.2	0.88179348	0.72981595	0.100529306
8	0.7	0.3	620	550	0.90942029	0.66871166	0.098441041
9	0.8	0.2	600	587.1	0.92753623	0.62319018	0.096731533
10	0.9	0.1	535	915.2	0.98641304	0.2206135	0.075292151
11	1	0	520	1095	1	0	0.062378207

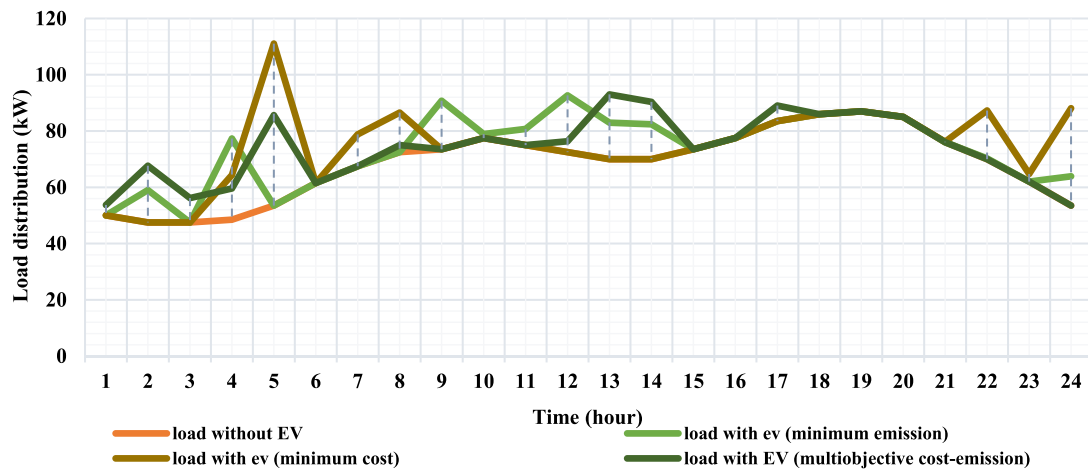


Fig. 25. Loading effect analysis for Scenario-III.

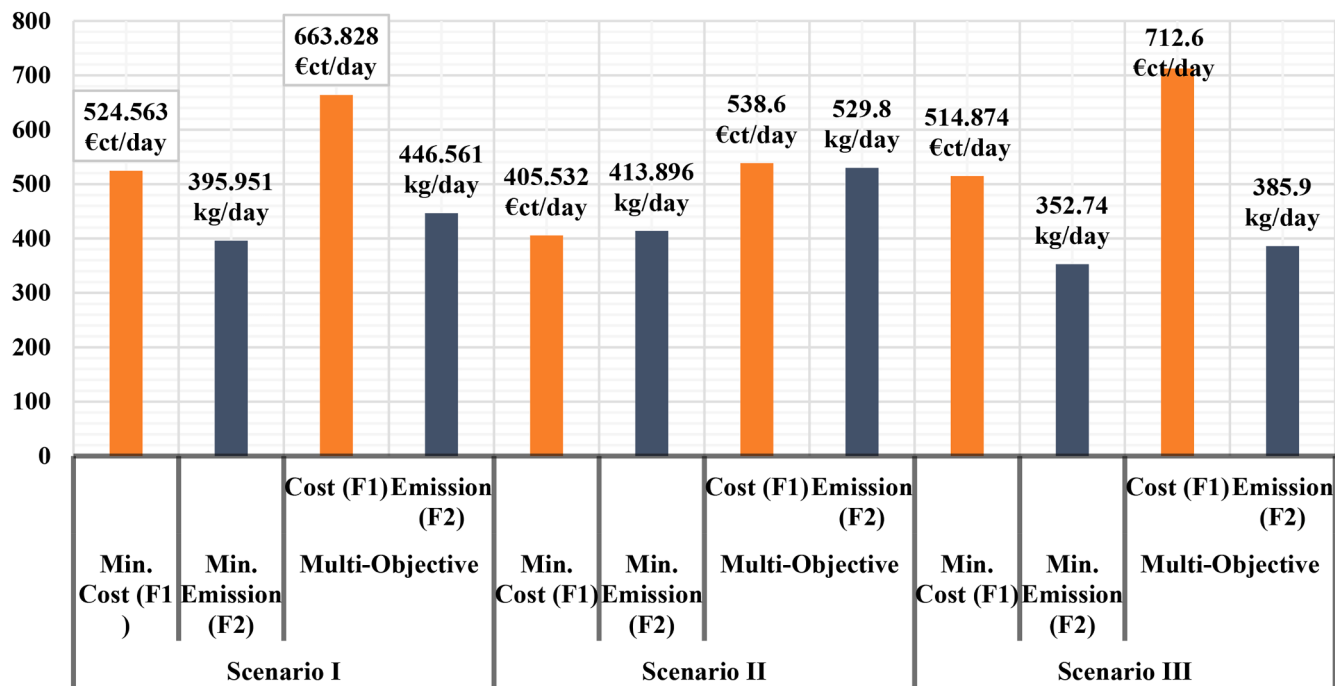


Fig. 26. Comparative analysis of lowest cost, lowest emission, and multi-objective cost-emission for three scenarios using SMA.

**Table 16**  
Battery-Size in kWh using SMA.

Operation Mode	Scenario-I	Scenario-II	Scenario-III
Operating Cost	103	164	107
Net Emission	113	206	159
Cost -Emission	144	125	156

high in relation to the power distribution, and vice versa. For instance, in Scenario-I, the minimal operating cost of power distribution using SMA is 524.563 €ct/day, but the corresponding emission is a staggering 912.68 kg/day. A similar tradeoff problem arises in the other cases as well. To provide a comprehensive analysis, Fig. 26 compares the lowest cost, lowest pollution emission, and multi-objective cost-emission outcomes; all determined using the SMA method in the presence of  $OM_{cost}$  and  $OCPD_{BESS}$  parameters across the three scenarios.

The negative battery icon on the power distribution graphs signifies that the battery is currently being recharged. Similarly, when the

utility's power consumption is negative, the MG sells electricity to the utility or main grid. After conducting an in-depth analysis of all of the minimum operational cost-related power distribution figures for Scenarios I, II, and III, it has become abundantly clear that MG obtains power from the grid for the first eight hours of the day. This is because, in the early morning hours of the day, the utility's electricity rate is less expensive than that of the other choices. However, the cost of power from the utility is fairly high mid-period of the day. Thus, the MG sells electricity to the grid mid-period of the day. Thus, there is a decrease in operational expenses. The power utilization profiles corresponding to the scenarios with minimized total emissions reveal that, given the zero-emission criteria, the predominant share of electricity has been drawn from PV and WT generation sources. Consequently, less power is drawn from the MT, FC, and BESS. It is also seen that MG delivers electricity to the utility during most of the day. In contrast, the multi-objective function-driven EM approach adopted for all three scenarios exhibits a more balanced power distribution, with medium-level contributions from the diverse DGs, BESS, and the utility grid. In this area, power is

**Table 17**

Operational cost results (€ct/day) with different population sizes using SMA.

	Population-size	Hits of achieving the best outcome	Average runtime of the simulation (sec.)	Best outcome	Mean outcome	Worst outcome
Scenario-I	10	25	0.976	524.57	524.573	524.59
	30	29	<b>1.001</b>	<b>524.563</b>	<b>524.564</b>	<b>524.601</b>
	50	29	1.035	524.563	524.564	524.601
	100	29	1.075	524.563	524.564	524.601
Scenario-II	10	24	1.0012	405.54	405.546	405.571
	30	29	<b>1.0015</b>	<b>405.5322</b>	<b>405.5342</b>	<b>405.5932</b>
	50	28	1.002	405.5322	405.5342	405.5932
	100	29	1.0034	405.5322	405.5342	405.5932
Scenario-III	10	25	1.0016	514.889	514.892	514.907
	30	29	<b>1.0018</b>	<b>514.8745</b>	<b>514.8753</b>	<b>514.8986</b>
	50	29	1.0021	514.8745	514.8753	514.8986
	100	29	1.0032	514.8745	514.8753	514.8986

**Table 18**

Emission results (kg/day) with different population sizes using SMA

	Population-size	Hits of achieving the best outcome	Average runtime of the simulation (sec)	Best outcome	Mean outcome	Worst outcome
Scenario-I	10	26	1.014	396.04	396.045	396.08
	30	29	<b>1.016</b>	<b>395.951</b>	<b>395.953</b>	<b>395.998</b>
	50	29	1.029	395.951	395.953	395.998
	100	29	1.045	395.951	395.953	395.998
Scenario-II	10	24	1.0131	413.95	413.959	413.998
	30	29	<b>1.0142</b>	<b>413.896</b>	<b>413.899</b>	<b>413.921</b>
	50	29	1.0152	413.896	413.899	413.921
	100	28	1.075	413.896	413.899	413.921
Scenario-III	10	25	1.0129	352.78	352.7815	352.789
	30	29	1.0131	352.74	352.7403	352.749
	50	27	1.0139	352.74	352.7403	352.749
	100	29	1.015	352.74	352.7403	352.749

**Table 19**

Comparison and research gap of previous work for the current research

References	Publication year	Formulation	Objective Function	WT and PV	BESS	Operational Cost	Emission	PHEV charging demand	OCPD <sub>BESS</sub>	OM <sub>cost</sub>
(Moghaddam et al., 2011)	2011	AMPSO	Multi	✓	✓	✓	✓	✗	✗	✗
(Milovanović et al., 2022)	2022	WHO	Multi	✓	✓	✓	✓	✗	✗	✗
(Kumar & Karthikeyan, 2024)	2024	GJO	Multi	✓	✓	✓	✓	✗	✗	✗
(Bahmani-Firouzi & Azizipanah-Abarghooee, 2014)	2014	Bat	Single	✓	✓	✓	✗	✗	✓	✓
(Yin et al., 2021)	2020	θ-MKH	Single	✓	✓	✓	✗	✗	✓	✓
(Sharma et al., 2016)	2016	QOSIMBO-Q	Single	✓	✓	✓	✗	✗	✓	✓
(Sharma et al., 2018)	2018	WOA	Single	✓	✓	✓	✗	✗	✓	✓
(Zandrazavi et al., 2022)	2022	MOPSO	Multi	✓	✓	✓	✓	✗	✗	✗
(Kavousi-Fard et al., 2014)	2014	θ-KH	Single	✓	✓	✓	✗	✓	✗	✗
(Li et al., 2021)	2021	GSA-PS	Single	✓	✓	✓	✗	✓	✗	✗
(Li et al., 2021)	2021	MSFLA	Single	✓	✓	✓	✗	✓	✗	✗
(Aldosary et al., 2021)	2021	θ-MKH	Single	✓	✓	✓	✗	✓	✗	✗
(Li et al., 2020)	2020	BSO	Single	✓	✓	✓	✗	✓	✗	✗
(Chakraborty & Ray, 2024)	2024	SMA	Multi	✓	✓	✓	✓	✗	✓	✓
Present article	–	SMA	Single and Multi both separately	✓	✓	✓	✓	✓	✓	✓

also sold throughout the midday hour. The optimum battery size obtained by SMA for each of the various power distribution techniques across every scenario is shown in Table 16.

After careful observation of load control graphs for three scenarios using SMA, it has been noticed that, during the operational cost minimization process, the extra load impact of PHEVs' charging is fulfilled during off-peak hours. In the same way, during the net pollution emission minimizing process, the extra load is fulfilled during peak and off-peak hours. For a multi-objective based cost-emission minimizing process, most of the extra load impact is fulfilled during off-peak hours. Sometimes, when an excess of energy is present at peak hours, the optimization process fulfills that extra load impact on that period.

The performance of the SMA and other algorithms was examined through 30 trial runs, showing the worst, average, and best outcomes.

Other methods that are employed to solve the same problem have a lower success rate than the SMA technique.

In SMA, the size of the population is a crucial tuning parameter that affects the total amount of respondents as well as the convergence rate and overall efficacy of the approach. Population size is also helpful to ensure the global optimal. Optimal results for cost or emission values are not achieved with excessively large or small populations. In this study, 30 trials were conducted for population sizes of 10, 30, 50, and 100, revealing that a population size of 30 produces the best outcomes. Population sizes larger than 30 showed minimal variation in operational costs and net emissions, while simulation time increased with larger populations. The SMA outcomes for operational cost and net emission reduction for various population sizes are shown in Tables 17 and 18.

## 7. Conclusion

This article focuses on determining the appropriate EM for an MG while taking into account the charging demands of PHEVs. The study explores three scenarios to emphasize the importance of the proposed EM process for the MG, particularly regarding the multi-objective solution concept. The analytical results for all three scenarios demonstrate that SMA yields better outcomes with a quicker convergence rate compared to GOA and SCA. Further analysis reveals that Scenario-II, where the BESS is initially charged to its maximum state and all DGs operate in a startup/shutdown mode based on economic preferences, achieves the better results using SMA, reducing operational costs by 20 % and 30 % compared to Scenarios I and II, respectively. Additionally, when examining emissions, Scenario-III—where the BESS holds the highest energy at the initial moment, and all DGs are kept in the startup (or "on") state—shows emission levels that are 10.91 % and 14.77 % lower than those in Scenarios I and II, respectively. A comparison of the multi-objective outcomes from SMA across the three scenarios clearly indicates that Scenario-III outperforms Scenarios I and II. This research presents significant advancements over existing literature, as outlined in Table 19. The loading effects of PHEVs are also examined, highlighting how an intelligent charging method distributes the additional load across different scenarios. The study concludes that a multi-objective EM process employing SMA effectively reduces costs and emissions while alleviating the strain from PHEV charging. These results enhance understanding of PHEV charging's influence on MG's EM and the effectiveness of multi-objective approaches. However, the research does not address vehicle-to-grid concepts, suggesting a potential avenue for future research to further improve MG efficiency and flexibility.

## CRediT authorship contribution statement

**Amit Chakraborty:** Writing – original draft, Visualization, Validation, Software, Resources, Project administration, Methodology, Investigation, Formal analysis, Data curation, Conceptualization. **Saheli Ray:** Writing – review & editing, Writing – original draft, Visualization, Validation, Supervision.

## Declaration of competing interest

The authors declare that they have no known competing financial interests or personal relationships that could have appeared to influence the work reported in this paper.

## Funding

Not applicable.

## Acknowledgements

Not applicable.

## Data availability

No data was used for the research described in the article.

## References

- Aghajani, G., & Ghadimi, N. (2018). Multi-objective energy management in a micro-grid. *Energy Reports*, 4, 218–225. <https://doi.org/10.1016/j.egyr.2017.10.002>
- Aghdam, F. H., Kalantari, N. T., & Mohammadi-Ivatloo, B. (2020). A chance-constrained energy management in multi-microgrid systems considering degradation cost of energy storage elements. *Journal of Energy Storage*, 29, Article 101416. <https://doi.org/10.1016/j.est.2020.101416>
- Alam, M. J. E., Muttaqi, K. M., & Sutanto, D. (2015). Effective utilization of available PEV battery capacity for mitigation of solar PV impact and grid support with integrated V2G functionality. *IEEE Transactions on Smart Grid*, 7(3), 1562–1571. <https://doi.org/10.1109/tsg.2015.2487514>
- Alarcón, M. A., Alarcón, R. G., González, A. H., & Ferramosca, A. (2022). Economic model predictive control for energy management of a microgrid connected to the main electrical grid. *Journal of Process Control*, 117, 40–51. <https://doi.org/10.1016/j.jprocont.2022.07.004>
- Aldosary, A., Rawa, M., Ali, Z. M., Latifi, M., Razmjoo, A., & Rezvani, A. (2021). Energy management strategy based on short-term resource scheduling of a renewable energy-based microgrid in the presence of electric vehicles using 0-modified krill herd algorithm. *Neural Computing and Applications*, 33, 10005–10020. <https://doi.org/10.1007/s00521-021-05768-3>
- Ali, Z. M., Al-Dhaifallah, M., Alkhalfaf, S., Alaas, Z., & Jamali, F. (2023). Optimal planning and design of a microgrid with integration of energy storage and electric vehicles considering cost savings and emissions reduction. *Journal of Energy Storage*, 71, Article 108049. <https://doi.org/10.1016/j.est.2023.108049>
- Bahmani-Firooz, B., & Azizipanah-Abarghooee, R. (2014). Optimal sizing of battery energy storage for micro-grid operation management using a new improved bat algorithm. *International Journal of Electrical Power & Energy Systems*, 56, 42–54. <https://doi.org/10.1016/j.ijepes.2013.10.019>
- Chakraborty, A., & Ray, S. (2024). Economic and environmental factors based multi-objective approach for optimizing energy management in a microgrid. *Renewable Energy*, 222, Article 119920. <https://doi.org/10.1016/j.renene.2023.119920>
- Chen, S. X., Gooi, H. B., & Wang, M. Q. (2011). Sizing of energy storage for microgrids. *IEEE transactions on smart grid*, 3(1), 142–151. <https://doi.org/10.1109/TSG.2011.2160745>
- Chen, T., Cao, Y., Qing, X., Zhang, J., Sun, Y., & Amaralatunga, G. A. (2022). Multi-energy microgrid robust energy management with a novel decision-making strategy. *Energy*, 239, Article 121840. <https://doi.org/10.1016/j.energy.2021.121840>
- Eskandari, H., Kiani, M., Zadehbagheri, M., & Niknam, T. (2022). Optimal scheduling of storage device, renewable resources and hydrogen storage in combined heat and power microgrids in the presence plug-in hybrid electric vehicles and their charging demand. *Journal of Energy Storage*, 50, Article 104558. <https://doi.org/10.1016/j.est.2022.104558>
- Fouladi, E., Baghaee, H. R., Bagheri, M., & Gharehpetian, G. B. (2020). Power management of microgrids including PHEVs based on maximum employment of renewable energy resources. *IEEE Transactions on Industry Applications*, 56(5), 5299–5307. <https://doi.org/10.1109/TIA.2020.3010713>
- Ghaedi, A., Dehnavi, S. D., & Fotohabadi, H. (2016). Probabilistic scheduling of smart electric grids considering plug-in hybrid electric vehicles. *Journal of Intelligent & Fuzzy Systems*, 31(3), 1329–1340. <https://doi.org/10.3233/JIFS-162199>
- Katiraei, F., Iravani, R., Hatziargyriou, N., & Dimeas, A. (2008). Microgrids management. *IEEE power and energy magazine*, 6(3), 54–65. <https://doi.org/10.1109/MPE.2008.918702>
- Kavousi-Fard, A., Abunarsi, A., Zare, A., & Hoseinzadeh, R. (2014). Impact of plug-in hybrid electric vehicles charging demand on the optimal energy management of renewable micro-grids. *Energy*, 78, 904–915. <https://doi.org/10.1016/j.energy.2014.10.088>
- Kumar, R. P., & Karthikeyan, G. (2024). A multi-objective optimization solution for distributed generation energy management in microgrids with hybrid energy sources and battery storage system. *Journal of Energy Storage*, 75, Article 109702. <https://doi.org/10.1016/j.est.2023.109702>
- Li, G., & Zhang, X. P. (2012). Modeling of plug-in hybrid electric vehicle charging demand in probabilistic power flow calculations. *IEEE Transactions on Smart Grid*, 3 (1), 492–499. <https://doi.org/10.1109/tsg.2011.2172643>
- Li, H., Rezvani, A., Hu, J., & Ohshima, K. (2021b). Optimal day-ahead scheduling of microgrid with hybrid electric vehicles using MSFLA algorithm considering control strategies. *Sustainable Cities and Society*, 66, Article 102681. <https://doi.org/10.1016/j.scs.2020.102681>
- Li, N., Su, Z., Jerbi, H., Abbassi, R., Latifi, M., & Furukawa, N. (2021a). Energy management and optimized operation of renewable sources and electric vehicles based on microgrid using hybrid gravitational search and pattern search algorithm. *Sustainable cities and society*, 75, Article 103279. <https://doi.org/10.1016/j.scs.2021.103279>
- Li, S., Chen, H., Wang, M., Heidari, A. A., & Mirjalili, S. (2020b). Slime mould algorithm: A new method for stochastic optimization. *Future generation computer systems*, 111, 300–323. <https://doi.org/10.1016/j.future.2020.03.055>
- Li, Y., Mohammed, S. Q., Nariman, G. S., Aljojo, N., Rezvani, A., & Dadfar, S. (2020a). Energy management of microgrid considering renewable energy sources and electric vehicles using the backtracking search optimization algorithm. *Journal of Energy Resources Technology*, 142(5), Article 052103. <https://doi.org/10.1115/1.4046098>
- Liang, X., Wu, D., Liu, Y., He, M., & Sun, L. (2021). An enhanced slime mould algorithm and its application for digital IIR filter design. *Discrete Dynamics in Nature and Society*, 2021(1), Article 5333278. <https://doi.org/10.1155/2021/5333278>
- Liu, X., Zhao, M., Wei, Z., & Lu, M. (2022). The energy management and economic optimization scheduling of microgrid based on Colored Petri net and Quantum-PSO

- algorithm. *Sustainable Energy Technologies and Assessments*, 53, Article 102670. <https://doi.org/10.1016/j.seta.2022.102670>
- Miao, D., & Hossain, S. (2020). Improved gray wolf optimization algorithm for solving placement and sizing of electrical energy storage system in micro-grids. *ISA transactions*, 102, 376–387. <https://doi.org/10.1016/j.isatra.2020.02.016>
- Milovanović, M., Klimenta, D., Panić, M., Klimenta, J., & Perović, B. (2022). An application of Wild Horse Optimizer to multi-objective energy management in a micro-grid. *Electrical Engineering*, 104(6), 4521–4541. <https://doi.org/10.1007/s00202-022-01636-y>
- Moghaddam, A. A., Seifi, A., Niknam, T., & Pahlavani, M. R. A. (2011). Multi-objective operation management of a renewable MG (micro-grid) with back-up micro-turbine/fuel cell/battery hybrid power source. *energy*, 36(11), 6490–6507. <https://doi.org/10.1016/j.energy.2011.09.017>
- Rezaee, S., Farjah, E., & Khorramdel, B. (2013). Probabilistic analysis of plug-in electric vehicles impact on electrical grid through homes and parking lots. *IEEE Transactions on Sustainable Energy*, 4(4), 1024–1033. <https://doi.org/10.1109/TSTE.2013.2264498>
- Sedighizadeh, M., Fazlhashemi, S. S., Javadi, H., & Taghvaei, M. (2020). Multi-objective day-ahead energy management of a microgrid considering responsive loads and uncertainty of the electric vehicles. *Journal of Cleaner Production*, 267, Article 121562. <https://doi.org/10.1016/j.jclepro.2020.121562>
- Sharma, S., Bhattacharjee, S., & Bhattacharya, A. (2016). Quasi-Oppositional Swine Influenza Model Based Optimization with Quarantine for optimal allocation of DG in radial distribution network. *International Journal of Electrical Power & Energy Systems*, 74, 348–373. <https://doi.org/10.1016/j.ijepes.2015.09.007>
- Sharma, S., Bhattacharjee, S., & Bhattacharya, A. (2018). Probabilistic operation cost minimization of Micro-Grid. *Energy*, 148, 1116–1139. <https://doi.org/10.1016/j.energy.2018.01.164>
- Tao, H., Ahmed, F. W., Latifi, M., Nakamura, H., & Li, Y. (2021). Hybrid whale optimization and pattern search algorithm for day-ahead operation of a microgrid in the presence of electric vehicles and renewable energies. *Journal of Cleaner Production*, 308, Article 127215. <https://doi.org/10.1016/j.jclepro.2021.127215>
- Yin, N., Abbassi, R., Jerbi, H., Rezvani, A., & Müller, M. (2021). A day-ahead joint energy management and battery sizing framework based on  $\theta$ -modified krill herd algorithm for a renewable energy-integrated microgrid. *Journal of Cleaner Production*, 282, Article 124435. <https://doi.org/10.1016/j.jclepro.2020.124435>
- Zandrazavi, S. F., Guzman, C. P., Pozos, A. T., Quiros-Tortos, J., & Franco, J. F. (2022). Stochastic multi-objective optimal energy management of grid-connected unbalanced microgrids with renewable energy generation and plug-in electric vehicles. *Energy*, 241, Article 122884. <https://doi.org/10.1016/j.energy.2021.122884>